

## MECHANISM OF SUCCESSIVE SOLVOLYTIC EXTRACTION OF COAL

D. K. Sharma and S. K. Singh  
Centre for Energy Studies,  
Indian Institute of Technology, Delhi  
Hauz Khas, New Delhi-110016, INDIA

**KEYWORDS:** Coal, Extraction, Solvents

Coal macromolecules are associated (interlocked and intermeshed) with each other so strongly that it generally requires stronger conditions for extraction or solubilization of more than 10-20% of coal. Extraction of coal in an organic solvent is an essential requirement for the conversion of coal to value added fuels and chemicals without a significant loss in original coal constitution and its energy. As a part of our large program on development of convenient and cost effective techniques for solvent extraction of coal under atmospheric pressure conditions using coal derived chemicals, work on successive extraction of coal using anthracene oil-quinoline (Qn) - liquid paraffin (LP) and anthracene oil (AO) - ethylenediamine (EDA) - liquid paraffin was undertaken. The procedure for the successive extraction of coal using different solvents for 24h extraction, has been reported earlier (1). In fact, Assam coal, Talcher coal and Neyveli lignite (analysis shown in Table 1) when subjected to successive solvent extraction (for 24h in each solvent), i.e., anthracene oil-ethylenediamine-liquid paraffin solvents showed 70% extraction of Assam coal, 59% extraction of Talcher coal, and 63% of Neyveli lignite. This was more than that observed using AO-Qn-LP solvents in successive extractions (Table-2) (1).

Table - 1: Analysis of Coals and Lignite

Proximate Analysis: On Dry Basis (%)

| Coal            | Moisture | Mineral Matter | Volatile Matter | Fixed Carbon |
|-----------------|----------|----------------|-----------------|--------------|
| Assam Coal      | 2.8      | 8.3            | 42.0            | 46.9         |
| Talcher Coal    | 2.1      | 16.9           | 38.8            | 42.2         |
| Neyveli Lignite | 8.7      | 6.1            | 46.6            | 38.6         |

Ultimate Analysis (% on Dry Mineral Matter Free Basis)

| Coal            | Carbon | Hydrogen | Sulfur | Nitrogen | Oxygen | Atomic H/C | O/C  |
|-----------------|--------|----------|--------|----------|--------|------------|------|
| Assam Coal      | 77.0   | 5.7      | 3.8    | 1.5      | 12.0   | 0.88       | 0.12 |
| Talcher Coal    | 74.8   | 5.3      | 1.0    | 1.6      | 17.3   | 0.87       | 0.17 |
| Neyveli-Lignite | 62.0   | 5.3      | 1.4    | 0.9      | 30.4   | 1.02       | 0.37 |

The observations showed that there are solvents which are capable of successively extracting coal resulting in 60-70% extraction of coal. In fact, maximum extraction of Assam coal was found to be in AO and this was 36%. This showed that a major portion of coal (64%) remains unextracted. The reason for this could be that the concentration gradient created by AO inside the solid coal and outside in the coal extract reaches a saturation stage and further

extraction in AO is not possible. This is the limit to which coal molecules can be associated with AO. Some of AO also gets into solid coal that is, it gets dissolved in coal. This mutual solubility is because of the reason that like dissolves like, as the major part of macromolecular and polyaromatic heterogeneous structure of coal resembles that of the constituents present in AO, especially phenanthrene and carbazole.

Table - 2: Successive Solvolytic Extraction of Coals Using AO-EDA-LP and AO-Qn-LP Solvent Systems

| Coal Sample     | Extractability (%) |     |    |    | Total Extraction Yield     |               |
|-----------------|--------------------|-----|----|----|----------------------------|---------------|
|                 | AO                 | EDA | QN | LP | On Original Coal Wt. Basis | On DMMF Basis |
| Assam Coal      | 33                 | 26  | *  | 28 | 65                         | 70            |
| Assam Coal      | 33                 | *   | 23 | 22 | 60                         | 65            |
| Talcher Coal    | 22                 | 25  | *  | 10 | 48                         | 59            |
| Talcher Coal    | 22                 | *   | 15 | 9  | 40                         | 48            |
| Neyveli Lignite | 30                 | 30  | *  | 21 | 61                         | 63            |
| Neyveli Lignite | 30                 | *   | 22 | 23 | 58                         | 60            |

\* This particular solvent was not used in the successive extraction  
 DMMF - Dry mineral matter free  
 Wt. - Weight

These studies showed that the structure of coal is flexible so as to hold solvent molecules between its molecules. In fact, this flexibility of intra and intermolecular bondings in coal molecules renders further extractable the residual coal obtained after AO extraction, in solvents such as Qn, EDA or LP. High boiling solvents such as LP (boiling range 330-350°C) are capable of energizing and stretching the coal macromolecules to such limits that these molecules are disintegrated and thus, reorient and repolymerize after extraction.

Flexibility of coal structure and mobility of loosened molecules is responsible for the successive extraction of coal in solvents having different chemical characteristics. In fact, coal has a heterogeneous structure having different structural units i.e., polyaromatic, hydroaromatic and paraffinic units linked through C-C, C-N-C, C-O-C and C-S-C linkages. The solvents having structural similarities with the structural units present in coal can easily dissociate and mobilize the coal molecules for their solution in that solvent. The extent of similarity between the structures of coal and that of the solvent and the boiling point of the solvent were generally found to determine the extent of extractability of coal.

The swelling ratio in Qn of the residual coal obtained after AO extraction was found to be more than that of the original coal (1). This showed that AO extraction results in reducing the degree of cross-linking in the structure of coal. However, extraction of coal in EDA or LP was found to result in an increase in the degree of cross-linking in the structure of coal, as revealed by the swelling studies. Probably, entrapment of EDA in coal would have resulted in the increase in the cross-linking in the structure of coal. LP extraction, being a high temperature extraction in a nonreactive and less interactive solvent, would result in the residual coal having a repolymerized cross-linked structure. The IR spectral studies of the residual coal obtained after the extraction of coal in AO or EDA or LP were found to show an increase in the aromatic character and a decrease in aliphatic character. The absorptions due to C=O group were missing in all the extracted coal residues obtained using AO or EDA or LP as a solvent. The percentage carbon and the atomic H/C ratios of the residual coals obtained after extraction in different solvents were also found to have been decreased in

comparison to those of the starting coal. This showed that coal might have undergone depolymerization, degradation and dehydrogenation as a result of extraction in AO, EDA or LP.

If the extraction results obtained after successive extraction in AO-EDA-LP solvents are analyzed then it can be seen that each solvent can extract its share of coal products that is structural moieties from coal which resemble its structure or properties. In fact, each solvent would extract the coal and would chemically depolymerize or degrade the coal for rendering it extractable in the next solvent of the successive extraction sequence to allow the extraction of increased amount of coal. The depolymerizing, degrading and molecular dispersing or dissociating ability of AO and EDA was found to be more than that of LP. In fact, preextraction with LP had an adverse effect on the successive extraction in AO or in Qn (1) or in EDA.

The point or position of attack i.e. chemical depolymerization or physical dissociation or dispersion of coal, by different solvents can be different depending upon the bond strength or the particular structural similarities between the coal and the solvent and of course, depending on boiling point of the solvent. Anthracene oil was found to be a wonder solvent for extraction of coal and for depolymerizing the coal (both chemically and physically) to render the enhanced amount of the (AO treated) residual coal in the next solvent, i.e., EDA, QN or LP. Orchin et al. (2) have reported the extraction studies on coals using different polynuclear aromatic compound such as phenanthrene, carbazole, pyrene, anthracene, fluoranthene, phenanthridine, fluorene, and diphenyl, etc. The actual three dimensional shape and size of the solvent molecule (especially angular arrangement of condensed aromatic rings instead of linear) were reported to be important factors for the ability of solvents to dissolve and disperse coal. Similarity of coal structure with angular ring phenanthrene type molecules (present in AO) allows the free passage (inside and outside) to these molecules inside the solid coal. This similarity of structures also helps in breaking the coal-coal (molecular) physical interactions such as London, vander Waals forces and H-bondings, by the solvents such as AO.

Since the coal structure is heterogeneous, therefore, a successive multiple solvent attack has been found to be a good way to loosen, unleash, unlock inter and intramolecular forces and disperse and to physically and chemically depolymerize the three-dimensional cross-linked gel structure of coal macromolecules for getting enhanced extraction without using any high pressure technique involving hydrogenation at elevated temperatures. Successive solvolytic extraction of coal affords a convenient and cost effective technique for solvent refining of coal under ambient pressure conditions.

#### Acknowledgements

The authors thank the Council of Scientific and Industrial Research, New Delhi, India for financial support.

#### References

1. Sharma, D.K. and Mishra, S., Energy and Fuels, **3**, 641 (1989).
2. Orchin, M., Golumbic, C., Anderson, J.E., and Storch, H.H., Bulletin 505, Bureau of Mines, United States Govt. Printing Office, Washington 1951.

## EFFECT OF MOISTURE ON THE SORPTION OF CO<sub>2</sub> BY COAL

V. C. Menon, C. A. Leon y Leon, T. Kyotani and L. R. Radovic  
Fuel Science Program  
Department of Materials Science and Engineering  
The Pennsylvania State University, University Park, PA 16802

Keywords: CO<sub>2</sub> Adsorption. Coal Swelling, Moisture Effects

### INTRODUCTION

It is well known that coal deposits contain varying amounts of moisture adsorbed or occluded within void spaces [1]. Coal seams are also known to contain varying amounts of gases such as methane and CO<sub>2</sub> [2]. Even though the presence of moisture is likely to reduce the gas storage capacity of coals [3,4], the reasons for such an occurrence are not well understood. Knowledge of the gas storage capacity of coals is of fundamental importance for coalbed methane studies. Therefore, it is of interest to investigate in detail the role of moisture in affecting the sorption of gases by coals. The presence of moisture in coals can affect the sorption of gases in the following ways: (a) gas dissolution; (b) pore blockage/filling; and (c) structural changes due to coal swelling. These effects have been addressed by (a) using CO<sub>2</sub> as sorbing gas (since it is present in coalbeds, it dissolves in water and it is often used to characterize the coal structure), and (b) using two coals having different swelling tendencies in water.

### EXPERIMENTAL

Table 1 shows the ASTM proximate and elemental analyses of the coals used in this study. In both cases, coal powders (-20 Tyler mesh) were studied under dry and moist conditions. Dry conditions were achieved by subjecting the samples to evacuation at ca. 10<sup>-3</sup> torr and 115°C overnight. Moist coals were prepared using an "incipient wetness" technique [5], which consisted in adding drops of distilled/deionized water to 1 g of coal and stirring until a muddy material remained. The amounts of water required

for achieving incipient wetness (Table 2) were 1.9 and 6.6 times greater than the equilibrium moisture contents for Mary Lee and (the more easily wetted) New Mexico coals, respectively.

Low pressure (0-830 torr) volumetric CO<sub>2</sub> sorption experiments were performed at 25°C using a Carlo Erba Sorptomatic 1800 apparatus. When moist samples were used, it was necessary to correct the equilibrium pressures for the contribution due to water evaporation. This was done by assuming that water evaporation reached equilibrium well within the time frame of the measurements. In addition, a further correction was applied to the CO<sub>2</sub> equilibrium pressure data to account for the amount of CO<sub>2</sub> dissolved in the water contained by the coal. In this case, both equilibrium CO<sub>2</sub> dissolution and the applicability of Henry's Law were assumed.

Moisture-induced swelling effects were assessed by performing experiments following a procedure described by Green et al. [6]. In essence, the volume expansion caused by the addition of water to 1 g of ~100 Tyler Mesh coals (after centrifugation) was measured, and was expressed as swelling ratios (Table 2).

## RESULTS AND DISCUSSION

**CO<sub>2</sub> Sorption Capacity of Dry vs. Moist Coals.** Figure 1 shows the CO<sub>2</sub> sorption isotherms for both dry and moist samples of Mary Lee and New Mexico coals. For both coals it is shown that the CO<sub>2</sub> adsorption capacity decreases in the presence of moisture. Similar results were reported for CO<sub>2</sub> sorption on lignites [3] and for CH<sub>4</sub> sorption on bituminous coals [4]. At very low relative pressures, the (typically concave downwards) shapes of the isotherms are affected by nonequilibrium conditions, as evidenced by the shapes of the respective Dubinin-Radushkevich (D-R) plots (Figure 2) [7]. The corresponding D-R equivalent surface areas for both dry coals (Table 2) are of reasonable magnitude compared to reported values [8]. Moist coals also provide D-R surface area estimates in close agreement with those of their dry counterparts (Table 2). Therefore, the equivalent CO<sub>2</sub> D-R

surface areas appear to be independent of the presence of moisture in the coals. Similarly, micropore volumes (obtained by extrapolation of D-R plots to saturation pressure) are comparable for both moist and dry samples of each coal. Hence, at pressures close to saturation the presence of moisture appears to have little bearing on the  $\text{CO}_2$  sorption capacity of coals. On the other hand, at low pressures there are clear differences in  $\text{CO}_2$  sorption capacity between dry and moist samples of each coal, with the latter taking up less  $\text{CO}_2$  than the former.

**Contribution by  $\text{CO}_2$  Dissolution to  $\text{CO}_2$  Sorption.** Figure 3 shows the variation in the calculated equilibrium amounts of  $\text{CO}_2$  dissolved in the moisture of each coal (assuming that the moisture consists of pure water) with  $\text{CO}_2$  partial pressure. These values, obtained using the amounts of water required to reach incipient wetness (Table 2), are seen to be very small in comparison with the total  $\text{CO}_2$  uptakes of each coal (Figure 3). Incipient wetness water values provide upper limits for the moisture contents of these coals, and are presumably comparable to the maximum moisture holding capacities of similar coals. Therefore, it is concluded that the dissolution of  $\text{CO}_2$  does not contribute significantly to the  $\text{CO}_2$  sorption by bituminous coals, at least at low relative pressures.

**Contribution by Pore Blockage/Filling to  $\text{CO}_2$  Sorption.** To account for the moisture-related decrease in  $\text{CH}_4$  sorption by bituminous coals, Joubert et al. suggested that some water molecules can effectively block pore entrances through specific interaction with oxygen functional groups in the coals [4]. These authors based their reasoning on the observation that the moisture-induced suppression in  $\text{CH}_4$  sorption (and in Langmuir equivalent  $\text{CH}_4$  surface area) was proportional to the oxygen content of the coals [4]. The same trend is observed for  $\text{CO}_2$  sorption in the present study (see Table 2 and Figure 1). However, the moisture-induced decrease in  $\text{CO}_2$  sorption in our case is independent of the D-R equivalent  $\text{CO}_2$  surface areas and, especially, the D-R micropore volumes of these coals (Table 2). The latter

observation suggests that the access of CO<sub>2</sub> to the coal pores is not restricted by the presence of moisture.

**Contribution by Coal Swelling to CO<sub>2</sub> Sorption.** Swelling ratios for the coals investigated differ significantly (Table 2), and are comparable to those reported for low rank coals [3,9]. In the presence of moisture, the more swelling coal, New Mexico, was found to experience a much more drastic reduction in CO<sub>2</sub> sorption capacity than the relatively non-swelling coal, Mary Lee (Figure 1). Studies of swelling-related structural changes in lignites using N<sub>2</sub> sorption [3] indicate that drying induces a collapse of macro- and mesopores, as well as undetectable changes in microporosity which parallel an increase in CO<sub>2</sub> sorption. The latter is in agreement with our observations at low relative pressures (Figure 1). Since CO<sub>2</sub> sorption at low pressures occurs by the preferential volume filling of the narrowest micropores (i.e., those with the highest sorption potentials) [7], the above results are best interpreted by postulating that the micropore diameters decrease upon drying. It follows that micropore diameters should increase when in contact with moisture, especially for swelling coals. This would explain why moisture limits the CO<sub>2</sub> sorption capacity of coals in the following way: (a) in the absence of moisture, CO<sub>2</sub> can penetrate and fill all accessible micropores; (b) in the presence of moisture, average micropore diameters increase, without necessarily involving a loss in micropore volumes (Table 2); (c) the increase in average micropore diameters limits the number of narrower pores that serve as sorption sites for CO<sub>2</sub> at low relative pressures, and hence causes a decrease in the low-pressure CO<sub>2</sub> sorption capacity of the coals (Figure 1); (d) the increase in average micropore diameters is more marked for swelling coals (Table 2), and consequently their CO<sub>2</sub> sorption capacity is more sensitive to the presence of moisture; (e) at higher relative CO<sub>2</sub> pressures, enough CO<sub>2</sub> is available to populate the wider micropores (i.e., those with lower adsorption potentials), and eventually at saturation conditions all accessible micropore volume is filled with CO<sub>2</sub> regardless of the presence of moisture.

## CONCLUSIONS

The CO<sub>2</sub> sorption capacity of two bituminous coals at low pressures (up to 830 torr) decreases in the presence of moisture. This contrasts the fact that their micropore volumes, obtained from the corresponding D-R plots, are comparable for both moist and dry coals. The contribution of CO<sub>2</sub> dissolution to its sorption was found to be negligible. The reduction in CO<sub>2</sub> sorption capacity is very significant for the more swelling coal compared to that of the less swelling coal. This remarkable reduction is possibly related to an increase in the average diameter of micropores as a result of swelling, rather than to blockage of pores by moisture.

## ACKNOWLEDGEMENTS

Support for this work was provided by the Gas Research Institute, Contract No. 5090-260-1987. The authors also thank Prof. B. McEnaney (University of Bath, U.K.) for helpful comments.

## REFERENCES

1. Nelson, C.R., in "Chemistry of Coal Weathering" (C.R. Nelson, Ed.), Elsevier, Amsterdam (1989), Ch.1.
2. Thimons, E.D. and Kissell, F.N., Fuel 52, 274 (1973).
3. Deevi, S.C. and Suuberg, E.M., Fuel 66, 454 (1987).
4. Joubert, J.I., Grein, C.T. and Bienstock, D., Fuel 52, 181 (1973).
5. Solar, J.M., Leon y Leon, C.A., Osseo-Asare, K. and Radovic, L.R., Carbon 28, 369 (1990).
6. Green, T.K., Kovak, J. and Larsen, J.W., Fuel 63, 935 (1984).
7. Linares-Solano, A., in "Carbon and Coal Gasification" (J.L. Figueiredo and J.A. Moulijn, Ed.), NATO ASI Series E-105, Dordrecht (1986), p. 167.
8. Mahajan, O.P., in "Coal Structure," Academic Press, New York (1982), p. 51.
9. Yost, R.S. and Creasy, D.E., Fuel 69, 648 (1990).

Table 1. Proximate and Ultimate Analyses of Coals Used

| PSU NUMBER              | PSOC 1469   | PSOC 1446      |
|-------------------------|-------------|----------------|
| SEAM NAME               | MARY LEE    | NEW MEXICO # 8 |
| STATE                   | ALABAMA     | NEW MEXICO     |
| COUNTY                  | WALKER      | SAN JUAN       |
| TOWNSHIP / CITY         | GOODSPRINGS | FRUITLAND      |
| RANK                    | HV bit. A   | HV bit. C      |
| PROXIMATE ANALYSIS      |             |                |
| % MOISTURE              | 1.9         | 11.2           |
| % ASH                   | 20.6        | 18.5           |
| % VOLATILES             | 27.3        | 33.5           |
| % FIXED CARBON          | 50.2        | 36.8           |
| ULTIMATE ANALYSIS (daf) |             |                |
| % CARBON                | 84.9        | 77.3           |
| % HYDROGEN              | 5.7         | 5.0            |
| % NITROGEN              | 1.8         | 1.6            |
| % SULPHUR               | 1.0         | 1.1            |
| % OXYGEN (diff.)        | 6.6         | 15.0           |

Table 2. Properties of Coals Used

| PSU NUMBER  | PSOC 1469 | PSOC 1446 |
|---|-----------|-----------|
| % OXYGEN (daf, diff.)                               | 6.6       | 15.0      |
| % EQUILIBRIUM MOISTURE                              | 7.2       | 12.1      |
| INCIPIENT WETNESS VOLUME (cc/g)                     | 0.14      | 0.80      |
| MICROPORE VOLUME (cc/g)                             |           |           |
| DRY   | 0.14      | 0.07      |
| MOIST (CORRECTED)                                   | 0.15      | 0.08      |
| BET N <sub>2</sub> SURFACE AREA (m <sup>2</sup> /g) |           |           |
| DRY   | 26        | 16        |
| CO <sub>2</sub> SURFACE AREA (m <sup>2</sup> /g)    |           |           |
| DRY   | 162       | 105       |
| MOIST (CORRECTED)                                   | 156       | 93        |
| MICROPORE SLIT WIDTH (nm)                           |           |           |
| DRY   | 1.8       | 1.4       |
| MOIST (CORRECTED)                                   | 1.9       | 1.8       |
| SWELLING RATIO                                      | 1.09      | 1.29      |

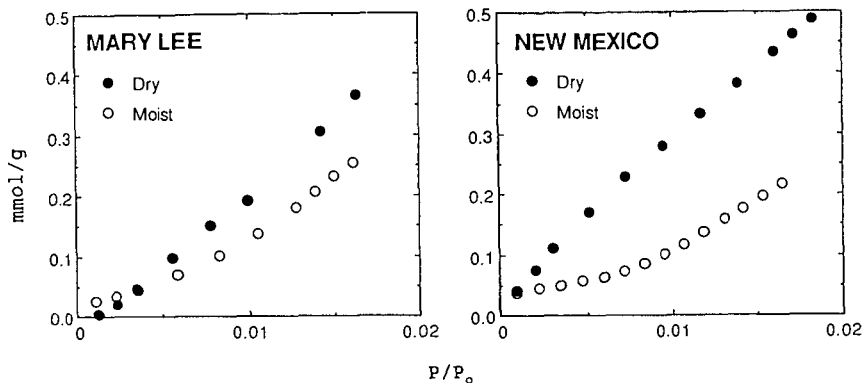


Figure 1. CO<sub>2</sub> adsorption isotherms.

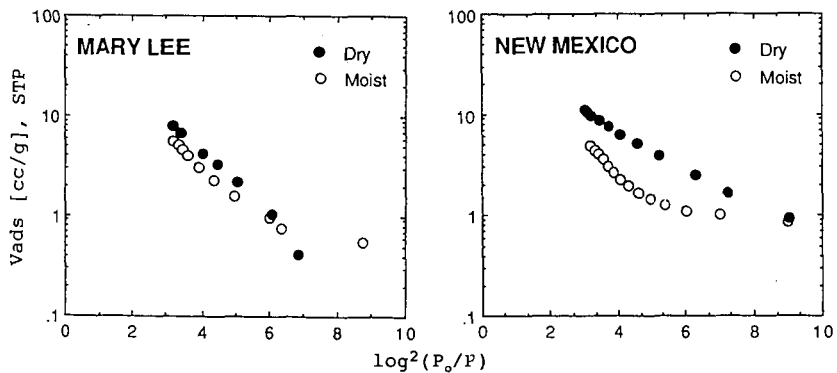


Figure 2. Dubinin-Radushkevich plots.

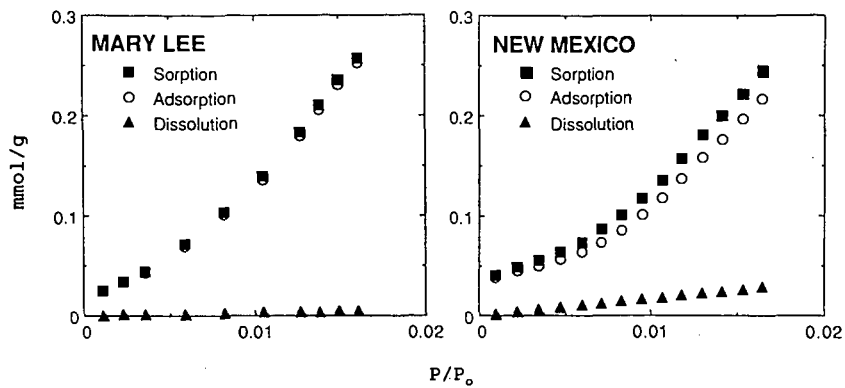


Figure 3. Contribution by dissolution to CO<sub>2</sub> sorption isotherms.

## CHARACTERIZATION OF INSOLUBLE ORGANIC MATTER ASSOCIATED WITH CLAY MINERALS FROM SYNCRUDE SLUDGE POND TAILINGS\*

Abdul Majid, Bryan D. Sparks and John A. Ripmeester  
National Research Council of Canada  
Institute for Environmental Chemistry  
Ottawa, Ontario, K1A 0R9, CANADA

Keywords: Syncrude Sludge, Insoluble Organic Matter, Humic Matter

Hot water extraction of bitumen from Alberta oil sands generates large quantities of tailings slurry. The fine grained sludge component of this waste is the most troublesome because of its stability and poor compaction potential. Dispersed bitumen, and organic matter that is insoluble in common solvents (IOM), are associated with the fines contained in these clay slimes. This organic matter is believed to be partly responsible for the intractability of the sludge, and it could therefore play an important role in determining the behavioural characteristics of oil sand slimes. In previous investigations we had attempted to enrich the insoluble organic matter by dissolving the minerals in concentrated HCl/HF. As a result of this treatment the inorganic material is decomposed, but the organic constituents are also likely to undergo significant changes. In the present work we have attempted a milder HCl/HF treatment for mineral dissolution. The results from the current investigation are compared with the results of the previous study to assess the chemical alterations of the organic matter resulting from the two treatments.

### INTRODUCTION

Hot water extraction of bitumen from Alberta oil sands generates large quantities of tailings slurry.<sup>1-4</sup> These tailings consist mainly of sand and an aqueous dispersion of various clay minerals, some of which are associated with significant amounts of insoluble organic matter (IOM).<sup>5-10</sup> This IOM is believed to be partly responsible for the intractability of the sludge and could therefore play an important role in determining the nature of slime stability.<sup>1,5</sup> It is believed that the IOM causes the clay particle surfaces to develop a hydrophobic character, allowing particle bridging, by means of residual bitumen, thereby setting up a weak gel structure.

In previous work, IOM from a number of oil sands tailing streams as well as oil sand feedstock samples has been isolated and characterized.<sup>5,7-9,11</sup> IOM was enriched by decomposing the inorganic material with concentrated HCl/HF, which might have resulted in the chemical alterations of the organic constituents. In this investigation we have attempted a milder HCl/HF treatment for mineral dissolution. The results from the studies using mild or severe extraction conditions have been compared in order to assess any chemical alterations that might have occurred during the deashing procedure.

### EXPERIMENTAL

Sample description and isolation procedure for organic rich solids fraction have been reported previously.<sup>9</sup>

HCl/HF Treatment Procedure. The general procedure for mineral dissolution and IOM enrichment is shown in Figure 1.

\* Issued as NRCC No. 32541

**NMR Measurements.** The solid state  $^{13}\text{C}$  NMR spectra were obtained at 75.47 MHz on a Bruker MSL-300 spectrometer, using a magic angle spinning (MAS) probe. For all samples a cross polarization technique was used with a contact time of 2 ms, and a repetition time of 1 s. Each spectrum was the Fourier transform of 1500-40,000 free induction decay curves.

## RESULTS AND DISCUSSION

Table 1 lists the yields for IOM and volatiles obtained during the mild as well as concentrated acid treatments. The ash content of the IOM is also listed.

**Table 1. Yields of IOM and Volatiles**

| Treatment         | Yield w/w % |           | Ash Content of IOM<br>w/w % |
|-------------------|-------------|-----------|-----------------------------|
|                   | IOM         | Volatiles |                             |
| Mild Acid         | 9.6         | 41        | 9                           |
| Concentrated Acid |             |           |                             |
| A                 | 24.7        | 60        | 35                          |
| B                 | 2.1         | 55        | 29                          |

Comparison of the results of mild acid treatment with those from the concentrated acid treatment indicates that the organic concentrate obtained from the former exhibited lower ash levels when compared to the concentrates produced by the latter treatment. This observation could result from a greater possibility of forming insoluble fluorosilicates during severe rather than mild acid treatment. Lower weight loss because of the volatiles in the mild acid treatment case as compared to the severe acid treatment case is also consistent with this interpretation.

**Elemental Analyses.** Elemental compositions of a sample of humic acid and IOM fractions obtained from both mild and severe acid treatments are compared in Table 2.

**Table 2. Elemental Analyses (dry, ash free basis)**

| Sample       | Treatment Scheme | Elemental Analyses |     |     |     |      | Atomic Ratios |      |
|--------------|------------------|--------------------|-----|-----|-----|------|---------------|------|
|              |                  | C                  | H   | N   | S   | O*** | H:C           | O:C  |
| Solids, 1-6* | Mild Acid        | 70.3               | 5.7 | 1.3 | 3.8 | 18.9 | 0.97          | 0.20 |
| Solids, 1-8* | Mild Acid        | 55.8               | 4.0 | 1.0 | 5.1 | 34.1 | 0.86          | 0.46 |
| IOM**        | Conc. Acid       | 69.1               | 6.5 | 0.7 | 5.6 | 18.1 | 1.12          | 0.20 |
| Humic Acid-1 | 2% NaOH          | 71.3               | 6.8 | 1.2 | 2.8 | 17.9 | 1.14          | 0.19 |

\* Figure - 1; \*\* Previous study ref. 9; \*\*\* By difference

The two IOM fractions obtained after mild acid treatment (solids, 1-6 and 1-8) had significantly different elemental compositions. Solids 1-6, the organic concentrate obtained from fraction 1-3, had an elemental composition resembling humic acid-1 and organic concentrate obtained previously<sup>9</sup> using severe acid treatment. The average elemental composition of these fractions (humic acid-1, solids 1-6 and IOM from severe acid treatment) are identical to those of the solvent extractable humic acids from Australian brown coal and benzene/methanol extracts from oil phase solids reported previously.<sup>5,12</sup> Elemental composition of the organic concentrate 1-8, obtained from fraction 1-4, appears to be similar to those reported for peat and soil humic matter.<sup>13,14</sup> Unlike the findings for the samples subjected to severe acid treatment<sup>5,9</sup> the present samples showed no trace of halogens.

Figure 2 is a van Krevelen diagram showing the humic acid and IOM fractions from both mild and severe acid treatments. All samples fall in the region of type III kerogen. Organic matter of type III kerogens is usually derived from plants of terrestrial origin and is rich in polyaromatic nuclei and heteroatomic ketone and carboxylic acid groups.<sup>15</sup> This type of organic matter is not considered to have any potential for hydrocarbon generation and usually matures to give coal. It is comparable in maturity to humic acids from lignite or subbituminous coals and is relatively immature when considered in light of its oil generation potential.<sup>7</sup>

**<sup>13</sup>C NMR Spectra.** The CP/MAS <sup>13</sup>C NMR spectra for a number of samples are shown on Figure 3. A comparison of these spectra indicates that resolution is equally improved for all samples, regardless of the carbon concentration. However, the spectral resolution in the carbohydrate region (50-100 ppm) is much better for solids 1-8 as compared with that for IOM, obtained using concentrated HCl/HF. This suggests that carbohydrates are less susceptible to attack by mild HCl/HF. Also, the peaks for aromatic carbons were sharper for solids 1-6 and 1-8 than in the spectrum for IOM obtained from concentrated acid treatment.

The aromaticity ( $f_a$ ) values for fractions 1-6 and 1-8 obtained using mild acid treatment are comparable to those for the IOM obtained from severe acid treatment (0.4 and 0.47 respectively Vs 0.44). These values are considerably higher than those reported for soil and aquatic humic acids and are comparable to those reported for humic acids from subbituminous coal and Victorian brown coal lithotypes.<sup>5,12</sup> As higher aromaticity is characteristic of a contribution from vascular plants<sup>16</sup>, it is likely that the humic matter associated with oil sands is largely derived from terrestrial sources.

## CONCLUSIONS

The results of this investigation are indicative of the presence of at least two different types of organic matter associated with oil sands solids. The two organic types had significantly different elemental compositions, with one fraction being almost identical to coal humic acids while the other was similar to peat and soil humic matter.

## ACKNOWLEDGEMENTS

The authors would like to thank H. Séguin and Ann Web for technical assistance with elemental analyses, and Dr. R. Schutte of Syncrude Canada Ltd. for providing a sample of sludge pond tailings.

## REFERENCES

1. Kessick, M.A. J. Can. Pet. Techn. 77, 49 (1979).
2. Camp, F.W. in 'The Tar Sands of Alberta, Canada', Cameron Engineering Inc., Denver, CO, USA, 1969.
3. Bakshi, N.N., Gillies, R.G. and Khare, P., Env. Sci. Techn. 9, 363 (1975).
4. Young, R.N. and Sethi, A.J., J. Can. Pet. Techn. 76, 76 (1978).
5. Majid, A. and Ripmeester J.A., Fuel 65, 1726 (1986).
6. Majid, A., Sirianni, A.F. and Ripmeester, J.A., Fuel 61, 477 (1982).
7. Majid, A. and Ripmeester J.A., 'Metal Complexes in Fossil Fuels: Geochemistry, Characterization and Processing', ACS Symposium Series 344, 290-306 (1987).
8. Majid, A. and Ripmeester J.A., Fuel 69, 1527 (1990).
9. Majid, A., Sparks, B.D. and Ripmeester J.A., Fuel 69, 145 (1990).
10. Ignasiak, T.M., Zhang, Q., Kratochvil, B. et al., AOSTRA J. Res. 2, 21 (1985).
11. Majid, A., Sparks, B.D. and Ripmeester, J.A., Fuel 70, 78 (1991).
12. Verheyen, T.V., Johns, R.B. and Blackburn, D.T., Geochim. Cosmochim. Acta, 46, 269 (1982).
13. Schnitzer, M. and Khan, S.U., "Humic Substances in the Environment", Marcell Dekker, New York, 1972.
14. Hartenstein, R., Science, 212, 743 (1981).
15. Tissot, B.P. and Welte, D.H. in "Petroleum Formation and Occurrence", Springer-Verlag, New York, USA, 1984.
16. Christman, R.F. and Gjessing, E.T., "Aquatic and Terrestrial Humic Materials", Ann Arbor Sci. Pub., Ann Arbor, 1983.

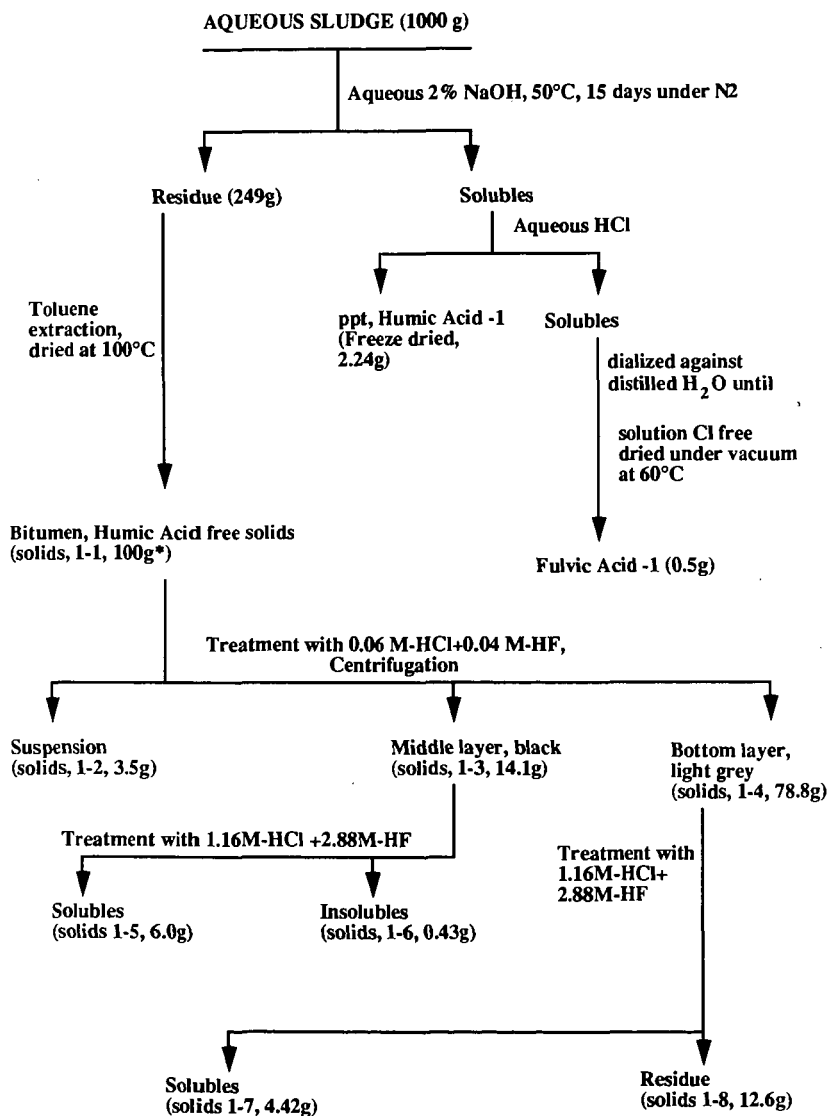


**Figure 1. Separation and mild HCl/HF acid treatment scheme**

\* Represents amount taken for further treatment and not actual yield.

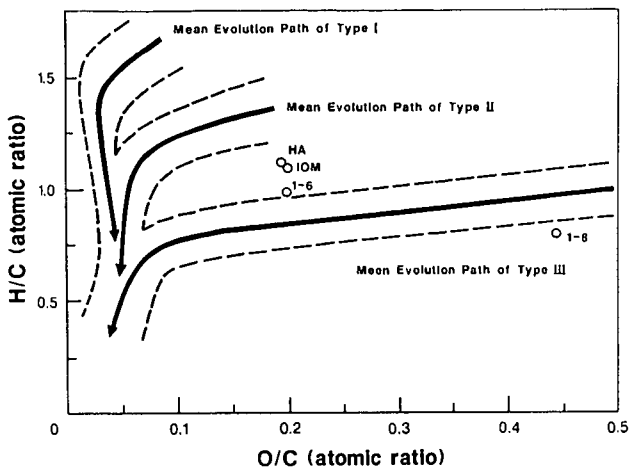


Figure 2. van Krevelen diagram showing the elemental composition of humic acid and organic matter concentrate fractions

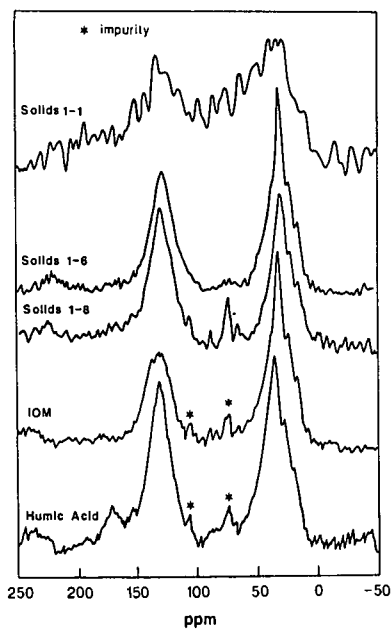


Figure 3. CP/MAS -  $^{13}\text{C}$  NMR spectra of various fractions from synchrode sludge pond tailings shown in Table 2

## Characterization of Humic Acids from Sludge Pond Solids\*

Abdul Majid, Bryan D. Sparks and John A. Ripmeester  
National Research Council of Canada  
Institute for Environmental Chemistry  
Ottawa, Ontario, K1A 0R9, Canada

Keywords: Humic Acids, Oil Sands, Sludge

Considerable quantities of organic material, insoluble in common organic solvents, are known to be associated with the inorganic minerals present in oil sands. This insoluble organic matter (IOM) consists of both humic and non-humic components. This organic matter is believed to be partly responsible for the intractability of the sludge. In our previous work we have successfully isolated non-extractable residual organic matter from oil sand tailings using oil phase agglomeration and acid dissolution techniques. In this investigation we have isolated humic acids from a number of samples of mineral solids obtained from Syncrude sludge pond tailings. These solids were obtained from sludge using different experimental conditions such as soxhlet extraction followed by air drying of solids and centrifugation followed by air drying or vacuum drying of solids. Humic matter was extracted from these solids using a mixture of  $\text{Na}_4\text{P}_2\text{O}_7$  and  $\text{NaOH}$  which extracts both humic acids as well as organometallic compounds. Extraction with  $\text{NaOH}$  yielded humic acids from this composite organic material. The various samples of humic acids isolated were studied using elemental analysis and  $^{13}\text{C}$  NMR spectroscopy.

### INTRODUCTION

Athabasca oil sand is a complex, variable mixture of bitumen, sand, water and clays. The hot water process used for the extraction of bitumen from oil sands produces large volumes of tailings, consisting mainly of sand and a dispersion of various clay minerals. Some of these clay minerals are associated with significant amounts of insoluble organic matter (IOM).<sup>1-7</sup> This insoluble organic matter consists of both humic and non-humic components and is believed to be partly responsible for the intractability of the sludge.

\* Issued as NRCC No. 32540

In our previous work we have successfully isolated non-extractable (toluene insoluble) residual organic matter from oil sand tailings using oil phase agglomeration and HCl/HF mineral dissolution techniques.<sup>4,8</sup> Characterisation of this organic material using elemental analysis and spectroscopic techniques was reported recently.<sup>3-5</sup> Based on those investigations it was suggested that the non-extractable organic material associated with oil sand minerals was mostly humic matter. This conclusion was also supported by the work of Ignasiak et al<sup>7</sup> who have reported that this organic matter consists of humic and non-humic components containing numerous oxygen functions.

In this investigation we have extracted humic acids from a number of samples of Syncrude sludge pond solids which had been treated under different experimental conditions. The various samples of humic acids isolated were studied using elemental analyses and <sup>13</sup>C NMR spectroscopy. The results of this study have been compared with the results obtained for the humic acids from oil sands feedstocks.<sup>9</sup>

### EXPERIMENTAL METHODS

**Materials.** The tailings pond sludge was provided by Syncrude Canada Ltd. A list describing the various samples subjected to humic acid extraction is shown in Table I.

Table I. Feedstocks description

| Sample ID | Sample Description                              | Ash (w/w %) | C (w/w %) |
|-----------|---|-------------|-----------|
| UTS       | Untreated sludge                                | -           | -         |
| TEODS     | Toluene extracted oven dried solids from sludge | 94.5        | 2.6       |
| ODS       | Oven dried untreated sludge                     | 85.4        | 5.3       |
| CWS       | Centrifuged wet solids from sludge              | -           | -         |
| CVDS      | Centrifuged vacuum dried solids from sludge     | 81.7        | 4.7       |

**Humic Acid Extraction.** Samples were first extracted using a mixture of 0.5 N NaOH + 0.1 M Na<sub>4</sub>P<sub>2</sub>O<sub>7</sub> to isolate composite organic matter consisting of a mixture of humic acids and organometallic compounds. This composite organic matter was then extracted with 0.1 N NaOH to isolate humic acids.

**Elemental Analyses.** Elemental analyses were performed using standard procedures reported previously.<sup>9</sup>

**NMR Measurements.** The solid state <sup>13</sup>C NMR spectra were obtained either at 45.28 MHz or at 75.47 MHz, using a magic angle spinning probe. For all samples a cross polarization technique was used with a contact time of 2-3 ms, and a repetition time of 1 s. Each spectrum was the Fourier transform of 1500-40,000 free induction decay curves.

## RESULTS AND DISCUSSION

Humic acids were extracted from a number of Syncrude sludge pond tailings samples that had been pretreated in accordance with the list shown in Table I. In Table II are listed the yield and ash content for each humic acid sample. The yield was calculated as weight percent of the total insoluble

Table II. The yield and ash content of humic acids

| Feedstock          | Humic Acid Yield<br>(w/w % of IOC*) | Ash Content of Humic<br>Acid (w/w %) |
|--------------------|-------------------------------------|--------------------------------------|
| UTS                | 21.7                                | 8.9                                  |
| TEODS              | 18.5                                | 55.3                                 |
| ODS                | 18.4                                | 1.6                                  |
| CWS                | 15.6                                | 2.8                                  |
| CVDS               | 19.7                                | 51.2                                 |
| Oil sands (Ref. 9) | 15.4 ± 9.4                          | 6.8 ± 5.8                            |

\* Insoluble organic carbon

organic carbon of the solids in the various samples. The amount of humic acid that could be extracted from various samples did not vary significantly (18.8±2%). Also, the amount of humic acids extracted from sludge samples compared with that extracted from oil sand feedstocks. This suggests that no significant quantities of humic matter could have been formed during oil sands processing or sludge storage and that the humic acids extracted from sludge solids could have been part of the humic matter associated with clay minerals of oil sands feedstock.

Ash content of the humic acid samples varied considerably. Humic acid samples extracted from TEODS and CVDS had the highest ash content of all the samples.

**Elemental Analyses.** The elemental analyses data are listed in Table III and can be summarized as follows:

Table III. Elemental Analyses of Humic Acids (w/w % dry, ash free)

| Feedstock          | Elemental Analysis |         |         |         |          | Atomic Ratios |           |
|--------------------|--------------------|---------|---------|---------|----------|---------------|-----------|
|                    | C                  | H       | N       | S       | O*       | H:C           | O:C       |
| UTS                | 71.3               | 6.8     | 1.2     | 2.8     | 17.9     | 1.14          | 0.19      |
| TEODS              | 56.3               | 5.8     | 0.8     | 1.3     | 35.8     | 1.24          | 0.48      |
| ODS                | 75.4               | 7.5     | 1.0     | 4.1     | 12.0     | 1.19          | 0.12      |
| CWS                | 66.6               | 4.5     | 1.5     | 1.6     | 25.8     | 0.81          | 0.29      |
| CVDS               | 66.2               | 6.9     | 1.7     | 2.8     | 22.4     | 1.25          | 0.25      |
| Oil Sands (Ref. 9) | 66±1.5             | 5.2±0.7 | 1.2±0.2 | 3.1±0.6 | 24.5±1.7 | 0.95±0.1      | 0.28±0.02 |

1. There was more variation in the elemental composition of humic acids extracted from Syncrude sludge pond tailings than those extracted from the oil sand samples reported previously.<sup>9</sup> This suggests that either the treatment of the samples of Syncrude sludge pond tailings has altered the humic matter eg. by oxidation or that the proportion of humic matter components extracted by a solution of Na<sub>4</sub>P<sub>2</sub>O<sub>7</sub>/NaOH varies from sample to sample.

2. The average elemental composition of these samples resemble those derived from coal and oil sand rather than those extracted from soil or marine sediments.<sup>9-11</sup>

**<sup>13</sup>C NMR spectra.** The solid state <sup>13</sup>C NMR spectra of the five humic acid samples extracted in this investigation are shown in Figure 1. The main features of these spectra are summarized below:

1. The NMR spectra of the samples derived from UTS and ODS have better spectral resolution than those of the other three samples. However, the spectral resolution does not appear to depend on the ash content of the samples.
2. None of the spectra showed any noticeable resonance in the carbohydrate region.
3. Only samples derived from ODS and CVDS had well defined resonances in the carboxylic region. Non-uniform distribution of carboxylic carbon could be due to the difficulties associated with its detection in these types of samples.
4. The aromaticities ( $f_a$ ) of the five humic acid samples ranged from 0.47 to 0.62. These values were comparable with previously reported values for humic matter fractions from oil sands.<sup>4,5,9</sup> However, these values are considerably higher than those reported for soil or aquatic humic acids. The higher values are closer to those reported for humic acids from victorian coal lithotypes.

#### ACKNOWLEDGEMENTS

The authors would like to thank Ann Webb and V. Clancy for technical assistance with elemental analysis and R. Schutte of Syncrude Canada Ltd. for providing a sample of sludge pond tailings.

## REFERENCES

1. Kessick, M.A., *J. Can. Pet. Techn.*, **77**, 49 (1979).
2. Majid, A., Sirianni, A.F. and Ripmeester, J.A., *Fuel*, **61**, 477 (1982).
3. Majid, A. and Ripmeester, J.A., *Fuel*, **65**, 1726 (1986).
4. Majid, A. and Ripmeester, J.A. 'Metal Complexes in Fossil Fuels: Geochemistry, Characterization and Processing', *ACS Symposium Series 344*, 1987, pp. 290-306.
5. Majid, A. Sparks, B.D. and Ripmeester, J.A., *Fuel*, **69**, 145 (1990).
6. Majid, A., Sparks, B.D. and Ripmeester, J.A., *Fuel*, **70**, 78 (1991).
7. Ignasiak, T.M., Zhang, Q., et al, *AOSTRA J. Res.*, **2**, 21 (1985).
8. Ripmeester, J.A. and Sirianni, A.F., *J. Can. Pet. Techn.*, **79**, 131 (1981).
9. Majid, A. and Ripmeester, J.A., *Fuel*, **69**, 1527 (1990).
10. Mossop, G.D. in 'Facts and principles of World Petroleum Occurrence', (Ed. A.D. Miall), *Can. Soc. Pet. Geol. Memoir*, **6**, 609-632 (1980).
11. Mossop, G.D., *Science*, **207**, 145 (1980).
12. Verheyen, T.V., John, R.B. and Blackburn, D.T., *Geochim. Cosmochim. Acta*, **46**, 269 (1982).

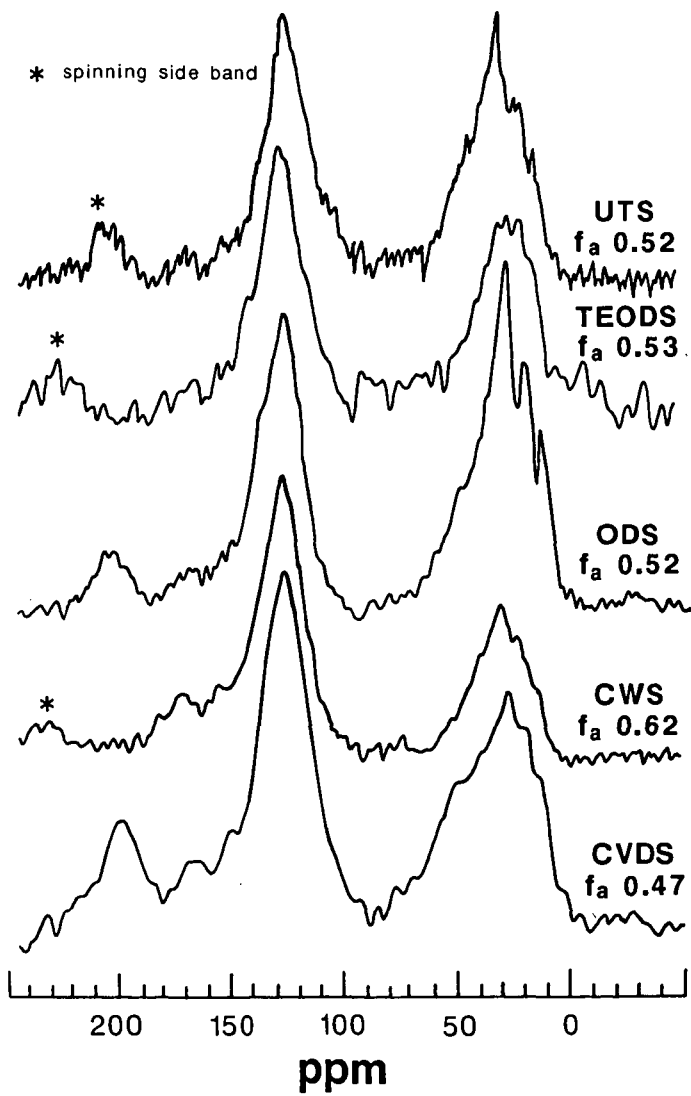


Figure 1. CP/MAS -  $^{13}\text{C}$  NMR spectra of humic acids

**A Thermal Swing Absorption Process  
for Production of Oxygen-Enriched Combustion Air**

S. Park, C. McLarnon, V.K. Mathur,  
S.A. Tomellini and R.P. Planalp\*

Chemistry and Chemical Engineering Departments  
University of New Hampshire  
Durham, NH 03824

**Keywords:** Oxygen separation, cobalt complex, thermal swing  
absorption

**Abstract.** A thermal swing absorption (TSA) process for the production of oxygen-enriched combustion air is described. The process is designed to achieve a ca. 50% fuel efficiency savings by the use of greater than 50% oxygen-enriched air in coal-fired boilers. The TSA process described has three components: an inorganic oxygen-carrying compound (carrier), a solution formulation of the carrier (with supports, promoters, and solvents), and a flow-system reactor with oxygen concentration monitoring. Criteria necessary to success of the process are identified. A literature search for appropriate compounds is summarized. Two compounds are identified, synthesized, formulated and tested in the TSA process. The compounds performed successfully over four absorption/desorption cycles. Goals for further improvements are stated.

**Introduction**

It is reported<sup>1</sup> that oxygen enriched combustion can substantially improve the thermal efficiency of a combustion system. Union Carbide found that in furnaces with combustion temperatures above 1100°C, an oxygen enrichment of 50 to 100% would result in a 40 to 60% fuel savings. The cost savings and thus economic feasibility of oxygen enriched combustion is sensitive to both fuel prices and the cost of producing oxygen. As an added advantage, the use of oxygen enriched combustion air (OECA) will also minimize NO<sub>x</sub> formation.

In a recent study<sup>2</sup> it is reported that thermal swing absorption (TSA) using a solution absorbent offers a potentially viable option for producing low cost OECA for industrial use. The TSA process consists of using a chemical in solution which is capable of absorbing oxygen at low temperature (say 23°C) and desorbing it at higher temperature (say 65°C). These temperatures can be obtained by cooling with ambient air and heating with flue gases. The use of waste heat from combustion gases would make this process economically very attractive.

A solution absorbent system consists of a reversible oxygen-binding chemical compound dissolved in a formulation of solvents and promoters. Four major criteria may be applied to the

absorbent solution. First, it should have a high, reversible and selective affinity for oxygen at room temperature or slightly above, and a lower affinity at a higher temperature (generally greater than 50°C), so that it will absorb and desorb oxygen. Second, the absorption process should happen at a reasonable rate. The solution should have a reasonable lifetime (i.e. it should be possible to cycle the absorbent many times without experiencing degradation). Finally, it should absorb the maximum weight of oxygen per unit weight of solution; this generally implies that the compound be quite soluble in the solvent and promoters.

It is important to note that while many compounds have been observed to have a reversible affinity for oxygen,<sup>3</sup> many physical properties of the compounds which affect their suitability for a TSA formulation are not known. Indeed, few solution absorbent TSA systems have been described.<sup>4</sup>

In this paper, we describe a literature survey of compounds for TSA formulation, and the identification of two compounds for study. The preparation, formulation, and testing of these two in a TSA apparatus is reported. Finally, the significance of the oxygen absorption performance and plans for the future are mentioned.

#### Experimental

**General.** Reagents and solvents were obtained from commercial sources (analytical reagent grade) and used as received. *N,N'*-bis(salicylidene) *o*-phenylenediimino cobalt(II) (also known as Salcophen or CoSalophen) was purchased from Aldrich Chemical Co. and used as received. NMR spectra were obtained on a Bruker AM-360 spectrometer. Infrared spectra were obtained on Perkin-Elmer 283B spectrometer.

**Preparation of *N,N'*-bis(salicylidene) ethylenediimino cobalt(II).**<sup>5</sup> I. *N,N'*-bis(salicylidene)ethylenediimine (salen). Freshly distilled salicylaldehyde (7.1 mL, 0.067 mol) in 95% ethanol (33 mL) was heated to a boil with stirring.

Ethylenediamine (2.2 mL, 0.0335 mol) was added and the solution was let cool. The resulting yellow precipitate (5.51 g, 61% yield) was filtered and dried under vacuum for 3 h. Proton NMR and elemental analysis (C, H, N) agreed with expected values.<sup>3</sup>

II. *N,N'*-bis(salicylidene) ethylenediimino cobalt(II) (Salcomine or CoSalen). Salen (2.74 g, 0.0102 mol) and sodium acetate (0.031 g) were dissolved in ethanol (31 mL), water (6.7 mL) and 1.0 M aqueous sodium hydroxide (24.3 mL). The mixture was brought to a boil with stirring and cobalt (II) chloride hexahydrate (2.43 g, 0.0102 mol) was added precipitating CoSalen as a brown product which was separated by filtration and washed with water until the washings were colorless. The cake was dried at 110°C for 3 h under reduced pressure, yield 2.75 g (83%). The elemental analysis (C, H, N) and IR spectrum (KBr pellet) agreed with expected values.

**Measurement of Oxygen Absorption Under TSA Conditions.** The measurement system is shown in Figure 1. Air (A) was passed through a needle valve and a calibrated Hastings mass-flow meter (B) to establish and measure the air flow rate. The air was bubbled through the reactor (D) where absorption and desorption take place. The effluent of the reactor was passed through an Infrared Industries IR-2200 Oxygen Analyzer (E) and then exhausted into a hood. A bypass line (C) around the reactor allowed for calibration and check of the analyzer. The reactor consists of an outer metal jacket around a glass reaction vessel fitted with a rubber stopper through which the gas inlet, gas outlet, thermometer and thermocouple were passed. The reactor was alternately cooled in each absorption cycle and heated in each desorption cycle. The gas inlet consisted of a glass line with a frit attached to promote contact of the gas with the liquid.

The data from the oxygen analyzer, mass flow meter, and thermocouple were collected using an IBM PC/XT with the labtech/Notebook data acquisition system. The amount of oxygen absorbed and desorbed was calculated by integrating the product of the oxygen concentration and flow rate over the cycle.

### Results and Discussion

**Selection of Candidate Compounds.** The literature was surveyed based on the above criteria, resulting in a tabulation of cobalt (II) compounds considered candidates for the TSA process. Table I is partial listing of these compounds.

Parameters found in the literature include the solvent and concentration of the formulation (columns 6 and 4). These are important to the fourth criterion above, because they provide information on the solubility of the cobalt complex. Clearly, those oxygen-binding compounds which are more soluble may produce a solution which contains more of the oxygen-binding ingredient and therefore has a greater oxygen absorbing capacity.

The nature of the axial base (column 5) affects the oxygen affinity of the complex (first criterion), by changing the electron density at cobalt, which is the active site for oxygen binding. Other parameters important to the first criterion are the temperature, binding ratio (mol Co:mol O<sub>2</sub>), and oxygen affinity (log K<sub>O<sub>2</sub></sub>). These parameters all provide information on how well the complex would hold and release oxygen during a TSA cycle.

These data are insufficient to determine if the compounds are suitable for the TSA process, however. Some of the data needed are oxygen affinities at higher temperatures (first criterion), maximum solubilities in a range of solvents (fourth criterion), rate of oxygen binding (second criterion), and stability to oxidative degradation (third criterion).

Compounds #1 and #2, CoSalen and CoSalophen (also referred to as salcomine and salcophen, respectively), were selected for further study to obtain some of the above data. They were chosen due to their relatively high oxygen affinities and reasonably

high solubilities. While DiCobalt-o-bistren, #4, has a higher oxygen affinity, its low concentration value of  $2 \times 10^{-4}$  M is not practical.

**Synthesis and Testing.** CoSalen was prepared by modification of a literature procedure while CoSalophen was purchased. CoSalen and CoSalophen were tested for solubility in various solvents. Dimethylsulfoxide (DMSO) was found to be most suitable, giving a high concentration, 0.03 M.

The formulations were tested in the TSA system, giving the results of Table II. In Table II, the first cycle for each compound may be disregarded, as the solutions were prepared in air so that the oxygen content of each solution at the start was unknown. Subsequent cycles give similar oxygen capacities in the absorption and desorption cycles, indicating that all oxygen bound is released. Thus, oxidative degradation is not occurring, because no oxygen is consumed in the cycles. Further, the oxygen capacities are similar from cycle to cycle, indicating that no other deterioration of the absorber is occurring over these cycles.

The utilization value indicates what fraction of the cobalt complex carries oxygen. This value is determined by the difference between the oxygen affinities at 65°C and 25°C, for CoSalophen (between the affinities at 65°C and 22°C for CoSalen). These are related to the  $\log(K_o)$  values of the complex.

Sample plots of oxygen absorption/desorption versus time are shown in Figures 2 (CoSalen) and 3 (CoSalophen), for the fourth cycle of each measurement. From these the rate of oxygen absorption and desorption may be approximated. For CoSalen, the absorption time is ca. 3 min and the desorption time ca. 4 min, while for CoSalophen it is ca. 4 min for absorption and 3.5 for desorption.

Future work will concentrate on improving the oxygen capacity of these TSA compounds. Several approaches will be taken. The solubility of the oxygen absorbing compound will be increased allowing a higher concentration of oxygen absorber per gram of solution. The utilization will be increased by increasing the desorption temperature and increasing the oxygen affinity of the compounds. Finally, the number of cycles will be increased to determine the lifetime of the compounds.

#### Conclusion

The thermal swing absorption process has been demonstrated using cobalt (II) Schiff-base complexes formulated as solution absorbents in a flow system. Parameters of the system have been determined for two cobalt complexes over four absorption/desorption cycles.

## References

1. Kobayashi, H., "Oxygen Enriched Combustion System Performance Study," Vol. 1, Technical and Economic Analysis, by Union Carbide Corp. for US DOE, March 1987.
2. Jain, R.C.; Keller, J.G.; Haq, Z. "Assessment of Thermal Swing Absorption Alternatives for Producing Oxygen Enriched Combustion Air," US DOE Office of Industrial Programs report, April 1990.
3. (a) Gubelmann, M.H.; Williams, A.F. *Struct. Bonding* 1983 55, 1. (b) Niederhoffer, E.C.; Timmons, J.H.; Martell, A.E. *Chem. Rev.* 1984 84, 137.
4. (a) Roman, I.C. "Absorption Process for Producing Oxygen and Nitrogen and Solution Therefor," U.S. Patent 4,451,270, May 1984 to Bend Research, Inc.; (b) Yamauchi, T. "Method for Oxygen Concentration," Japanese Patent JP 62-83302, issued April 16, 1987 to Taiho Industry Co. Ltd., Tokyo, Japan.
5. This preparation is adapted from the literature: Diehl, H.; Hach, C.C. *Inorg. Syn.* 1950 3, 196.

Table I. Candidate Compounds for Oxygen Production by the TSA Process

| No | Chemical (A) (Mol.Wt.)                            | Structure (A) | Conc. of (A)         | Axial base (B)   | Solvent (C)       | Temp (°C) | Ratio (Co:O <sub>2</sub> ) | gO <sub>2</sub> /g(A) | gO <sub>2</sub> /g soln. (A+B+C)                | log KO <sub>2</sub>              | Ref. # |
|----|---|---------------|----------------------|--|-------------------|-----------|----------------------------|-----------------------|---|----------------------------------|--------|
| 1  | CoSalen (325)                                     |               | 0.01M                | 4-Methylpyridine (2M)  | diglyme           | 25°       | 2:1                        | 0.0492                | 1.7x10 <sup>-4</sup>                            | 0.91                             | 1,2    |
| 2  | CoSalophen (377)                                  |               | 0.012M               | 4-Mepy (2M)<br>4-CNpy (1M)<br>Py (2M)<br>DMAP (2M)           | "                 | 25        | 1:1<br>2:1                 | 0.0849<br>0.0424      | 4.098x10 <sup>-4</sup><br>2.05x10 <sup>-4</sup> | -2.74<br>-2.82<br>-2.81<br>+1.04 | "      |
| 3  | CoOCH <sub>3</sub> Salen (355)                    |               | 0.010M               | 4-MePy (3M)  | "                 | 10        | 1:1                        | 0.0901                | 3.4x10 <sup>-4</sup>                            | -1.68                            | "      |
| 4  | DiCobalt- <i>o</i> -Bistren (645)                 |               | 2x10 <sup>-4</sup> M | NaOH   | H <sub>2</sub> O  | 25        | 1:1                        | 0.0496                | 6.4x10 <sup>-6</sup>                            | 4.57                             | 3      |
| 5  | Co(S-Me)en(NO <sub>3</sub> ) <sub>2</sub> (358.8) |               | 0.075M               | Et <sub>2</sub> en (2M)                                      | Formamide         | 25        | 1:1                        | 0.0892                | 3.49x10 <sup>-4</sup>                           | No data                          | 4      |
| 6  | 2,4,6-Tri(mesityl)-phenol (448)                   |               | 0.0372M              | 0.3g K <sub>2</sub> C <sub>2</sub> O <sub>7</sub> butanolate | <i>i</i> -butanol | 20        | 1:1                        | 0.07142               | 1.47x10 <sup>-3</sup>                           | No data                          | 5      |

References: 1. Martell, A.E. *Inorg. Chem.*, 1987, 26, 1026-1030; 2. Martell, A.E. *Inorg. Chem.*, 1989, 28, 3647-3652; 3. Meehan, R.J., Martell, A.E. *Inorg. Chem.*, 1988, 27, 7719; 4. Sauer, I.C. "Absorption Process for Producing Oxygen and Nitrogen and Solution Precipitation," U.S. Pat. #4,311,270, issued to Taino Industry Co. Ltd., Tokyo, Japan; 5. Yamachi, T. "Method for Oxygen Concentration," Japanese Patent JP 62-83302, issued April 16, 1987 to Taino Industry Co. Ltd., Tokyo, Japan.

Table 11. Oxygen Absorption Data

| Compound   | Conc. mol/L | Solution Mass, g | Cycle No. | Bath Temperature, °C |        | Oxygen Capacity, $\times 10^{-4}$ g(O <sub>2</sub> )/g(soln) |        | mol(O <sub>2</sub> )/mol(Compound) Absorp | Utilization, mol(O <sub>2</sub> )/mol(Compound) Desorp |
|------------|-------------|------------------|-----------|----------------------|--------|--|--------|---|--|
|            |             |                  |           | Absorp               | Desorp | Absorp   | Desorp |   |  |
| Cosalen    | 0.03        | 218              | 1         | 22                   | 65     | 0.890  | 1.54   | .110                                      | .191   |
| Cosalen    | 0.03        | 218              | 2         | 22                   | 65     | 1.81   | 2.00   | .225                                      | .249   |
| Cosalen    | 0.03        | 218              | 3         | 22                   | 65     | 1.80   | 1.90   | .224                                      | .235   |
| Cosalen    | 0.03        | 218              | 4         | 22                   | 65     | 1.81   | 1.83   | .225                                      | .227   |
| Cosalophen | 0.03        | 219              | 1         | 25                   | 65     | 5.05   | 1.15   | .063                                      | .144   |
| Cosalophen | 0.03        | 219              | 2         | 25                   | 65     | 1.26   | 1.29   | .158                                      | .162   |
| Cosalphen  | 0.03        | 219              | 3         | 25                   | 65     | 1.16   | 1.30   | .145                                      | .163   |
| Cosalphen  | 0.03        | 219              | 4         | 25                   | 65     | 1.15   | 1.23   | .142                                      | .153   |

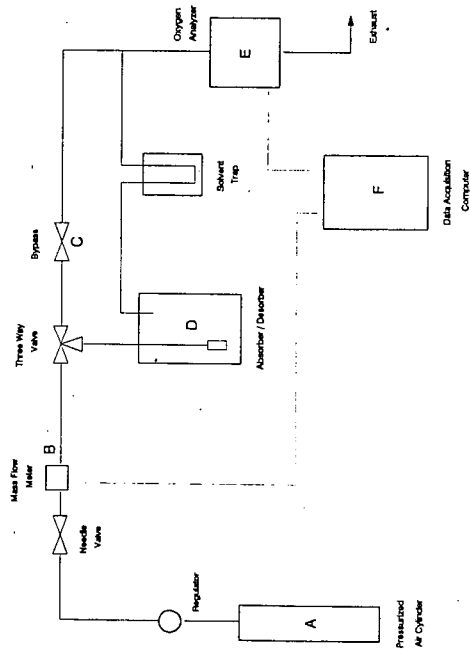


Fig. 1: Oxygen Absorption / Desorption Experimental Set-up

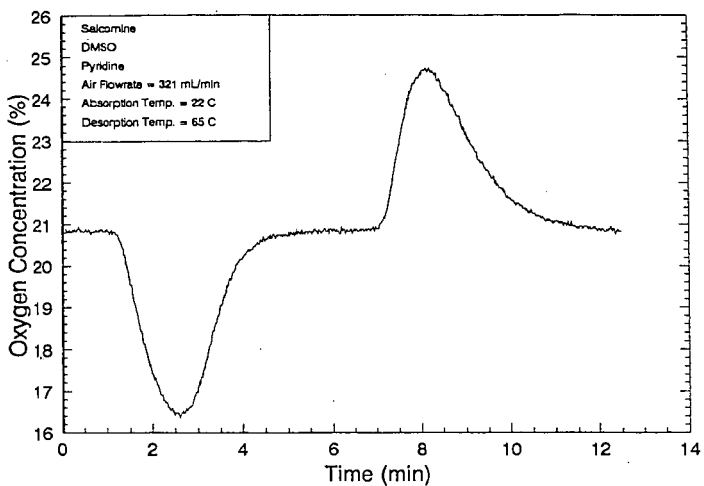


Fig. 2: Oxygen Absorption / Desorption for Salcomine

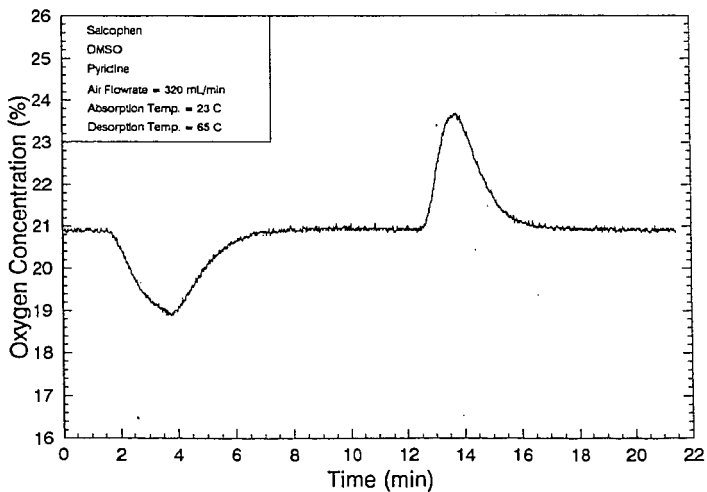


Fig. 3: Oxygen Absorption / Desorption for Salcophen

## Methanol and Carbon Monoxide Production from Natural Gas

Terry E. Helton, Jin-Woo Chun and Rayford G. Anthony  
Department of Chemical Engineering  
Kinetics, Catalysis and Reaction Engineering Laboratory  
Texas A&M University  
College Station, TX 77843

### INTRODUCTION

Partial oxidation of methane to methanol and formaldehyde holds considerable potential for producing liquid fuels and petrochemicals from natural gas. Several groups (Burch et al., 1989; Gesser et al., 1985 and 1987; Hunter et al., 1990; Yarlagadda et al. 1988) have investigated homogeneous partial oxidation. Various sensitizers were capable of lowering the partial oxidation reaction temperature (Hunter et al., 1987, 1990). For most of the literature cited, the methanol selectivity varies from 20 to 80 percent. Some research groups have stated that it is difficult to obtain consistent results for the direct conversion of methane into methanol. In this study we present data illustrating the importance of the closure of the oxygen balance, the effect of materials of construction and type of reactor on the yields and selectivity of methanol. A kinetic model containing 175 homogeneous free radical reactions was developed and is used to simulate the performance of a plug flow reactor. Helton (1991) presents additional details on this study.

### EQUIPMENT

Two reactor systems are utilized research to study the effects of reactor design on methane activity and product selectivity. Reactor system I can be operated from 1 - 100 atmospheres at temperatures between 25 and 450 °C. Non-selective catalytic wall effects are minimized by using a Pyrex liner. The tubular reactor and Pyrex liner is described in Figure 1. All tubing, exposed to temperatures above 180 °C contains an inner lining of fused silica in order to minimize the potential for surface reaction. For this system the feed is mixed and flows over several feet prior to entering the heated reactor zone of 400+ °C. In the reactor zone it is partial heated prior to entering the reactor tube through the 90 ° elbows. The elbows are 316 stainless steel and a portion of the SS is exposed to the reactants at high temperatures. Some or possibly even substantial reaction may have occurred in this section of the reactor.

Reactor system II is a commercial unit constructed by Autoclave Engineers, and is the Model 900 Micro-Scale Bench-Top Reaction System including the chromatographic system. Three basic modules comprise the reactor system: reactor, control, and analytical modules. A temperature controlled oven encloses the reactor system. Figure 2 provides a detailed description of the tubular reactor. For this system the gases are mixed at 180 °C and pass through an array of valves prior to entering the end of the reactor tube at 180 °C. No reaction occurs below 300 °C. As the fluid flows through the reactor tube it is heated by the three zone heater. The reaction is not conducted under isothermal conditions in either system, so that temperatures reported herein are the maximum temperatures of the reaction mixture. The analytical system

consists of an AE computer-controlled high-performance gas chromatograph containing a capillary and three packed columns along with a palladium transfer tube for hydrogen detection. Detailed operating procedures for the AE 900 Micro-Scale Bench-Top Reaction System exists in the manufacturer's operations manual.

The differences in the two reactor systems is the exposure of SS in the inlet elbows of Reactor System I and the possibility of reaction in this inlet section. Reactor System II has a straight section and no exposure of the reactants to SS as the reactants are heated to the reaction temperature. Also, with the AE-MSBTR instantaneous instead of time average material balances could be obtained.

#### RESULTS AND DISCUSSION

Burch et al. (1989) concluded the reason the high selectivity work of Gesser et al. (1987) could not be reproduced was due to small, but possibly important, differences in the design of the reactor. Burch and co-workers believed the methane to methanol gas-phase reaction operated within essentially unsteady-state conditions. Gesser et al. (1987) states that the reaction can occur under cool flame conditions in certain temperature and pressure regions. Also, the degree of pre-mixing of the reactant gases may have influenced the high selectivities reported.

Although the product distribution may be affected by the type of experimental apparatus, non-steady state conditions, or gas pre-mixing, failure to close the atom balances may explain the discrepancies in the range of selectivities observed in previous work. Figure 3, which was generated by using Monte Carlo simulation for a feed containing methane and 2.3% and 9.4% oxygen, respectively, illustrates the importance in closing carbon and oxygen atomic balances. For a feed containing 2.3% oxygen and 97.7% methane, a deviation in the carbon atom balance closure of 1% could result in 12 percentage points error in the methanol selectivity.

Table 1 illustrates that the addition of 5 percent ethane to the reaction mixture does not alter the methanol selectivity. However, the reaction temperature is lowered approximately 20 °C. Thus, ethane is capable of initiating the generation of free radicals more readily than methane which leads to further oxidation and enhances the formation of methanol at a lower temperature.

Figure 4 compares the methanol selectivity for the TEHBTR and AE-MSBTR reactor systems. The initial oxygen concentration was varied from 4.3 percent to 10.0 percent. Table 2 lists the gas hourly space velocity and reactor residence time for each reactor system. Except for one experiment, the residence time was maintained at approximately 17 seconds by varying the space velocity at each reaction pressure. The total pressure ranged from 20 to 50 atmospheres. Figure 4 indicates that methanol reaches a maximum after 20 percent of the oxygen is converted. The methanol selectivity could not be increased above 35 percent despite the range of oxygen concentrations and total pressures studied. There is an increase in methanol selectivity to 42 percent for reactor system TEHBTR, but this only occurred at an oxygen concentration of 4.3 percent, 20 atmospheres pressure, and a residence time of approximately 6 seconds.

The walls of the TEHBTR system appear to be catalytically active. When the total pressure is increased from 20 to 50 atmospheres the methanol selectivity decreases drastically from 30 to approximately 10 percent. If the partial oxidation of natural gas was purely homogeneous an increase in reactor pressure should minimize any surface reactions since the gas density to reactor wall surface is greater. Since the opposite is observed, the walls in the TEHBTR system must be catalytically active.

Few kinetic models for the homogeneous partial oxidation of methane to methanol have appeared in the literature. Onsager et al. (1989) and Durante et al. (1989) presented gas phase models at the International Chemical Congress of Pacific Basin Societies for the low temperature partial oxidation of methane to methanol. Onsager's reactor consisted of a one-chamber reactor with an alumina and stainless steel inner surface. The main part of the reaction rate parameters were taken from Tsang (1987) and Tsang and Hampson (1986). Some reactions were generated by Onsager et al. (1989) without any reference to literature values. The rate parameters of these reactions were estimated on the basis of analogous reactions.

Durante et al. (1989) constructed a kinetic model for the homogeneous gas phase reactions involved in methane partial oxidation utilizing published rate constants and activation parameters by Bedeneev et al. (1988). The model predicted the experimental findings of Yarlagadda et al. (1988) for runs at low temperature and oxygen partial pressures, but it could not reproduce the high methanol selectivities (exceeding 80 percent) reported at an 8 percent methane conversion. Onsager et al. (1989) and Durante et al. (1989) limited their models to the reaction of methane and oxygen. Thus, it was necessary to develop a model which incorporated the combined reactions of methane and ethane with molecular oxygen.

A kinetic model consisting of 175 free radical reactions was developed to simulate the reported experimental results. Pre-exponential constants for five reaction steps were increased above the recommended literature values in order to predict the experimental data. The pre-exponential constants were multiplied by the factors illustrated in Table 3. The published rate constants for these two reactions were estimated from the analogous reaction of formaldehyde with molecular oxygen. The increased pre-exponential constants for the formation of carbon dioxide is within the uncertainty of the literature values. Figure 5 shows a comparison of model predictions with experimental data. The kinetic model predicts the experimental data with remarkable accuracy.

#### CONCLUSIONS

Oxygen atom balance closure is needed to insure a minimum error in the calculated methanol selectivities, because it is the limiting reactant when excess methane is used. Large deviations in products selectivities can occur even though the overall material and the carbon atom balance closures are satisfied to a  $\pm 2\%$ .

The proposed kinetic reaction mechanism is capable of predicting the homogeneous reaction of methane and ethane with molecular oxygen. The model accurately predicts the product selectivities and conversions for the range of experiments in this investigation.

Additional cracking reactions need to be added to the mechanism in order to predict higher ethylene selectivities at low oxygen conversions (less than 10 percent). This would lower the predicted formaldehyde selectivity at low conversions and help in predicting the formaldehyde selectivity more accurately. Also, some spectroscopic work could be performed to determine the free radical concentrations during the reaction. Since the free radicals appear to reach a pseudo steady state, spectroscopic instruments may be able to observe and quantify these species. This would help in improving the kinetic model.

#### ACKNOWLEDGEMENT

This research was supported in part by a grant from the Texas Advanced Technology Program.

#### LITERATURE CITED

- Bedeneev, V.I., M.Y. Gol'denberg, N.I. Gorban, and M.A. Teitel'boim, *Kinetika i Kataliz*, 29(7), 1 (1988).
- Burch, R., G.D. Squire, and S.C. Tsang, *Journal of the Chemical Society, Faraday Transactions I*, 85(10), 3561, (1989).
- Durante, V.A., D.W. Walker, W.H. Seitzer, and J.E. Lyons, 1989 *International Chemical Congress of Pacific Basin Societies, Preprints of 3B Symposium on Methane Activation, Conversion, and Utilization*, Honolulu, Hawaii, (1989).
- Gesser, H.D., N.R. Hunter and C.B. Prakash, *Chemical Reviews*, 85(4), 235 (1985).
- Gesser, H.D., N.R. Hunter, L.A. Morton, P.S. Yarlagadda and D.P.C. Fung, *American Chemical Society Preprints*, 32(3), 255 (1987).
- Helton, T.E., Ph. D. Dissertation, Department of Chemical Engineering, Texas A&M University (1991), Research Advisor: R. G. Anthony.
- Hunter, N.R., H.D. Gesser, L.A. Morton and P.S. Yarlagadda, *American Chemical Society, Division of Petroleum Chemistry Preprints*, 779 (1987).
- Hunter, N.R., H.D. Gesser, L.A. Morton, P.S. Yarlagadda and D.P.C. Fung, *Applied Catalysis*, 57(1), 45 (1990).
- Onsager, O.T., P. Soraker, and R. Lodeng, 1989 *International Chemical Congress of Pacific Basin Societies, Preprints of 3B Symposium on Methane Activation, Conversion, and Utilization*, Honolulu, Hawaii (1989).
- Tsang, W., *Journal of Physical and Chemical Reference Data*, 16(3), 471, (1987).
- Tsang, W. and R.F. Hampson, *Journal of Physical and Chemical Reference Data*, 15(3), 1087, (1986).
- Yarlagadda, P.S., L.A. Morton, N.R. Hunter and H.D. Gesser, *Industrial and Engineering Chemical Research*, 27, 252 (1988).

Table 1: Effect of Ethane on Reaction Temperature and Methanol Selectivity

| 94 % Methane              |                      | 89 % Methane - 5 % Ethane |                      |
|---------------------------|----------------------|---------------------------|----------------------|
| Reaction Temperature (°C) | Methanol Selectivity | Reaction Temperature (°C) | Methanol Selectivity |
| 413                       | 33.3                 | 388                       | 36.1                 |
| 421                       | 33.4                 | 390                       | 34.7                 |
| 429                       | 31.8                 | 398                       | 31.0                 |
| 421                       | 33.9                 | 401                       | 32.5                 |
| 414                       | 34.3                 | 405                       | 32.0                 |

Table 2: Experimental Conditions for TEHBTR and AE-MSBTR

| Reactor Conditions     | Unit    | Space Velocity, hr <sup>-1</sup> | Space Time, seconds |
|------------------------|---------|----------------------------------|---------------------|
| 4.3% Oxygen<br>20 atm  | TEHBTR  | 4652                             | 5.9 - 6.3           |
| 6.35% Oxygen<br>50 atm | AE-MBTR | 4165                             | 16.4 - 17.9         |
| 8.20% Oxygen<br>20 atm | AE-MBTR | 1573                             | 17.9 - 18.8         |
| 9.40% Oxygen<br>50 atm | AE-MBTR | 4165                             | 17.2 - 17.6         |
| 9.70% Oxygen<br>50 atm | TEHBTR  | 4200                             | 18.0 - 18.9         |
| 9.70% Oxygen<br>50 atm | AE-MBTR | 4165                             | 17.5 - 17.7         |
| 10.0% Oxygen<br>50 atm | TEHBTR  | 4104                             | 18.2-19.0           |

s

Table 3: Enhancement Factors for the Pre-exponential Constants

| Reaction   | Enhancement Factor |
|--|--------------------|
| $\text{CH}_4 + \text{O}_2 = \text{CH}_3 + \text{HO}_2$                   | $1.0 \times 10^7$  |
| $\text{C}_2\text{H}_6 + \text{O}_2 = \text{C}_2\text{H}_5 + \text{HO}_2$ | $7.0 \times 10^6$  |
| $\text{CO} + \text{CH}_3\text{O} = \text{CH}_3 + \text{CO}_2$            | 3.5                |
| $\text{CO} + \text{OH} = \text{CO}_2 + \text{H}$                         | 3.5                |
| $\text{CO} + \text{HO}_2 = \text{CO}_2 + \text{OH}$                      | 3.5                |

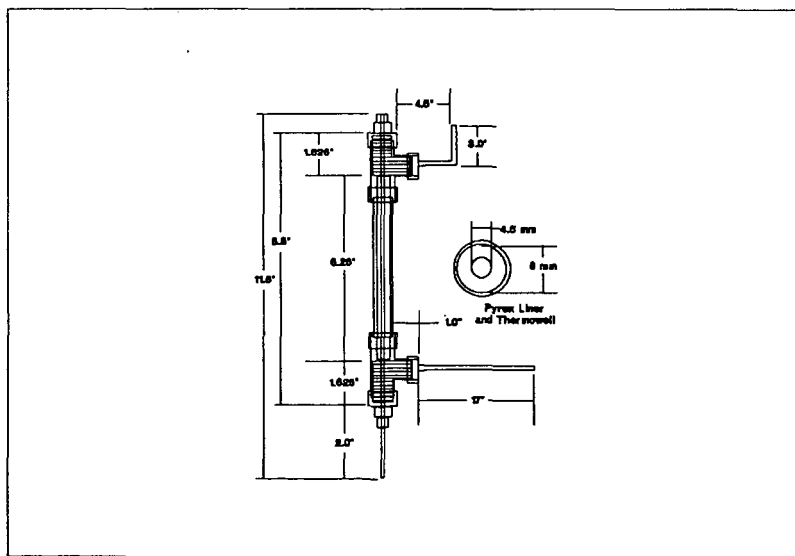


Figure 1: TEHBTR-Reactor Dimensions

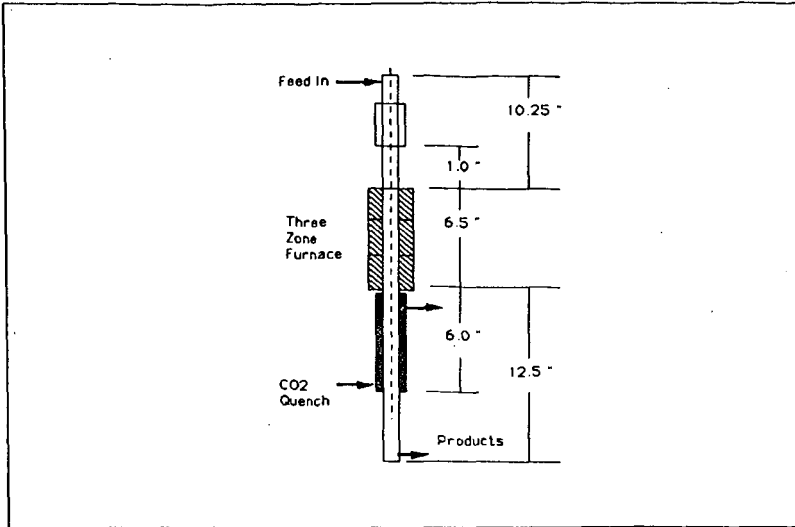


Figure 2: AE-MSBTR-Reactor Dimensions

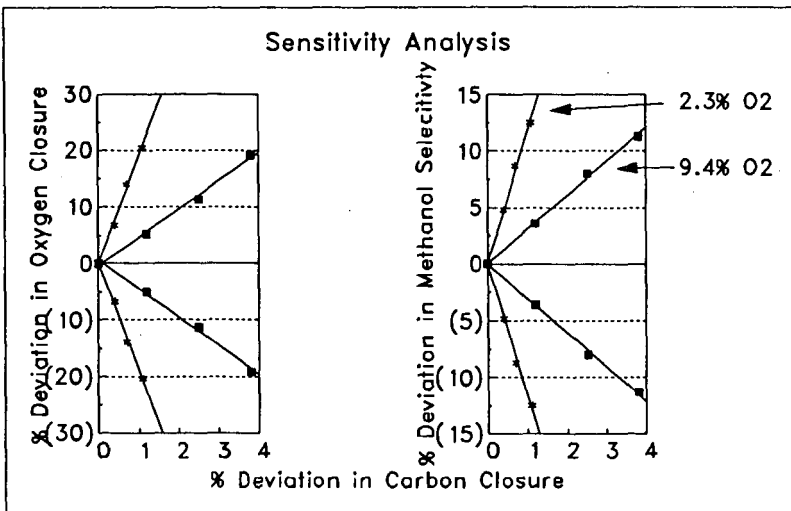


Figure 3. Monte Carlo Sensitivity Analysis (Oxygen feed concentrations of 2.3% and 9.4%)

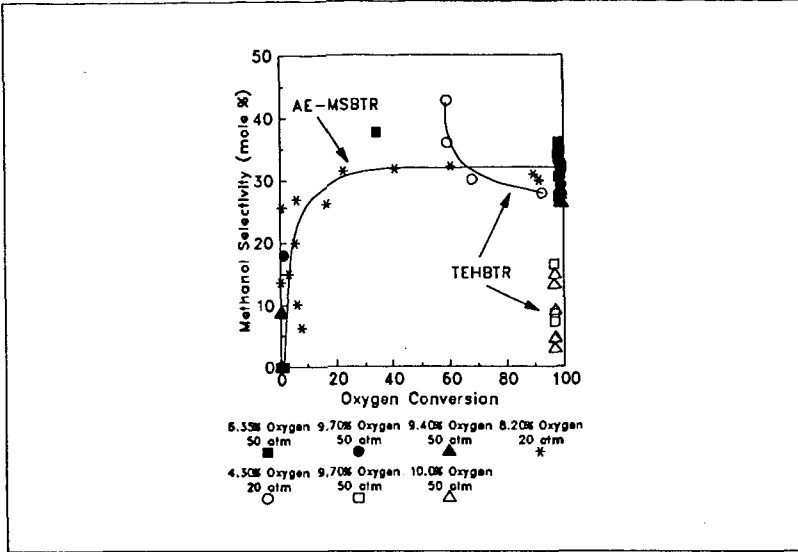


Figure 4: Methanol Selectivity for the Thermal Partial Oxidation of Natural Gas

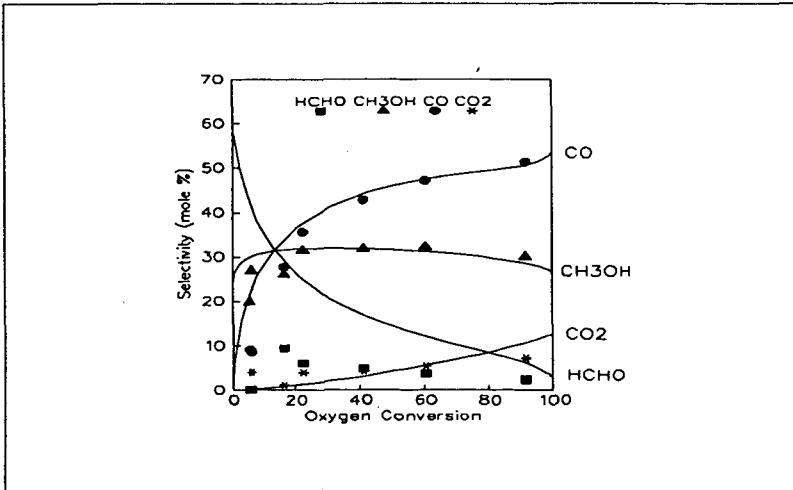


Figure 5: Comparison of Model Selectivity Predictions and Experimental Data for the Partial Oxidation of Natural Gas (8.2 % Oxygen, 5.1 % Ethane, 86.7 % Methane, Pressure = 20 atmospheres, Space Velocity = 1573 hr<sup>-1</sup>)

**SURFACE CHEMICAL STUDIES OF "HOT CORROSION LIFE PREDICTION MODEL FOR MARINE GAS TURBINE BLADES AND GUIDE VANES"**

Dasara V.Rathnamma,  
Code 2842, David Taylor Research Center  
Annapolis, MD, 21402-5067

R.Nagarajan  
IBM Corp, 5600 Cottle Road, San Jose, CA 95193

**Key words:** Hot Corrosion, chemical equilibrium,  
chemically frozen boundary layer,

**ABSTRACT**

The results of a theoretical program of research directed towards the study of hot corrosion in the hot gas pathways of marine gas turbines burning vanadium contaminated liquid fuels are presented here. A life prediction model, Life, is developed for turbine blades and guide vanes based on the application of fundamental heat, mass, and momentum transfer principles to the chemically reactive non-isothermal combustion environment. The corrosion rate is assumed to be limited by high Schmidt number diffusional dissolution of a protective oxide species into the condensed molten salt solution (equilibrium composition is predicted by means of free energy minimization by the computer program). Alloy surface effects are included to quantitatively relate predicted coating removal rate to hot corrosion data which are used to verify the validity of our theoretical approach. The physical insight into the mechanism of hot corrosion obtained through the study is expected to provide far reaching implications for the future design and protection of marine turbine components.

**INTRODUCTION**

Fuel composition, among other things, controls the corrosion and hence the life of airfoil material in the marine gas turbine engine. The use of fuels containing contaminants like sulfur, sodium, vanadium and sea salts, is known to cause rapid degradation of alloy coatings as well as substrate alloys of the blades and vanes. Molten salt mixtures of sulfates, vanadates and other hot corrosive species such as oxides of vanadium and sulfur formed as fuel combustion products dissolve the protective oxide on the blade surface. During fluxing a variety of complex chemical reactions take place which required analysis by computer-based multicomponent equilibrium algorithms. The high-Schmidt number Brownian diffusion limited oxide dissolution by the deposited liquid has been assumed to be the rate-limiting process in hot corrosion. Each of these processes has been characterized thoroughly and rigorously. The corrosion rate increases with the salt deposition rate, but the relationship is nonlinear and depends on the composition of the salt and the

substrate alloy or coating. Sodium as a fuel impurity or as airborne sea salts in the marine atmosphere condenses as sodium sulfate ( $\text{Na}_2\text{SO}_4$ ) and causes corrosion. In the temperature range 600-800°C, low temperature, hot corrosion is very sensitive to  $\text{SO}_2$  partial pressures in the gas phase. In the range 800-950°C, high temperature, hot corrosion is not quite as sensitive to  $\text{SO}_2$  levels. A theoretical model (1,2) for hot corrosion limited blade life based on the rates at which oxide formation and dissolution phenomena proceed, has been developed from theoretical considerations by the use of computer programs (3,4,5). The predictive computer program is called Life. The predicted effect of variations in operating parameters and surface coating oxides on predicted blade life has been studied.

Blade surfaces are usually coated with metal alloys that form an adherent, refractory and corrosion-resistant oxide layer on the gas side of the coating. Rosner and Nagarajan (6) have proposed the following mechanism for initiation and propagation of hot corrosion: at locations where the protective oxide scale is partially leached or completely dissolved by the condensed molten salt-'solvent', the metal substrate is more accessible, and hence vulnerable to catastrophic corrosion. Local saturation of the liquid layer is prevented by dynamic fluxing due to aerodynamic and centrifugal-shear forces which convey dissolved oxide from the site of dissolution to the tip and trailing-edge regions of the blade. The oxide dissolution rate is taken to be limited by high-Schmidt number Brownian diffusion of the oxide species in the melt (as well as by salt/oxide interfacial detachment kinetics). Other parameters that play a role in the oxide dissolution rate include aerodynamic variables such as the convective flux of the gas phase alkali contaminants, and material integrity characteristics of the blade alloy surface.

Many studies have been concerned in the literature with deposition mechanisms, the composition of the salt deposits (7) and mechanisms of low temperature hot corrosion (8). But our model for predicting the life of air foils, is based on fundamental principles. Objective of the present work is to understand the interfacial chemistry of the deposition and corrosion processes approach.

#### STEPS IN THE ANALYSIS

1. Equilibrium thermodynamic prediction of condensed liquid and vapor phase compositions (3).
2. Chemically Frozen Boundary Layer (CFBL) model prediction of deposition rates (4,5).
3. Estimation of physico-chemical properties of the molten salt solution.
4. Estimation of physical properties and parabolic oxidation rate constants of coating alloys.
5. Prediction of protective oxide coating dissolution rates into the condensed liquid 'solvent'.
6. Prediction of blade 'life' based on the competing dynamics of

oxide layer formation and dissolution.

Each of these steps, along with the assumptions inherent in each was previously addressed (1).

## RESULTS AND DISCUSSION

High temperature hot corrosion mechanisms reported in literature (7,8) are not based on rate studies. Model reported in this paper is a rate study model and it uses the multicomponent chemical vapor deposition (CVD) theory (9,10).

Local thermochemical equilibrium calculations by use of solution capable free energy minimization computer programs i.e., Complex Chemical Equilibria Calculations (CEC) of the National Aeronautics and Space Administration (NASA) and Package code of the Department of Energy (DOE) are shown in figures 1 and 2. Mole fractions of the product species depend upon the impurity concentrations in the fuels (table 1).

Figure 1. CEC predicted dominant vapor species.

Figure 2. Condensed liquid solution comprising principally of  $\text{Na}_2\text{SO}_4(1)$ ,  $\text{Na}_2\text{V}_2\text{O}_6(1)$ , and  $\text{V}_2\text{O}_5(1)$ .

Figure 3. Shows dependence of the CFBL computed deposition rate on surface temperature and fuel/air ratio.

At sufficiently low surface temperatures, the solution deposition rate is insensitive to surface temperature. As the solution dew point is approached, deposition rate drops to zero at the dew point. The dew point of the solution is in general, higher than that for any of the individual species. This dew point elevation effect, in combination with the freezing point depression effect and eutectic formation, considerably broaden the unsafe temperature range in which the deposit remains molten. For this reason, solution condensates are typically corrosive over a wider operating regime than pure condensates.

Molten salt deposition rate increases with an increasing fuel-to-air ratio, increasing gas main stream temperature, and with increasing sodium/vanadium concentrations in the combustion mixture. Pressure and sulfur level are predicted to have relatively insignificant effects on the computed deposition rate.

Figure 4. Shows dependence of oxide dissolution rate on blade surface temperature. Oxide dissolution rate can actually increase with temperature, even though the salt deposition rate drops rapidly. Oxide dissolution rate is predicted to increase with increasing fuel-to-air ratio, increasing gas mainstream temperature, and increasing sodium/vanadium gas phase concentrations. The rate as with deposition is insensitive to

pressure and sulfur level under normal turbine operating conditions.

Figure 5. Shows for pure metallic oxide coated turbine blades there is a monotonic increase in blade life with temperature since sulfidation corrosion only is considered as the life limiting factor. This inconsistency is due to omission of oxidation corrosion as also life limiting.

Figure 6. Predicts maximum blade life at the temperature when the sulfidation corrosion and oxidation corrosion intersect approximately at 1120K.

Figure 7. Shows evaluation of three Navy test fuels with regard to their corrosion potential. Below 1200 K, use of GT 10 would result in longer blade life than GT 12. NSFO (Navy special fuel oil) is a highly contaminated fuel not used in gas turbine engine.

Figures 8 and 9. Show life of blade material coated with several single metal oxides mostly.

Figure 10. Shows life of blade coated with typical metallic alloys and dependence of life on temperature.

#### CONCLUSIONS

Objective, central to the preliminary approach was accomplished. There is reasonable agreement between the model predictions and some of the experimental results reported in literature (11). The model needs improvement. Thermodynamic data on vanadium-oxygen gaseous species is lacking (12) in the thermodynamic data base (13,14). Ideal solution calculations are to be replaced by real solution calculations using the SAGE program which is a modified and improved version of sol-gas-mix program.

#### REFERENCES

1. Rathnamma, D. V. and R. Nagarajan, "Hot Corrosion Life Prediction Model for Marine Gas Turbine Blades and Guide Vanes" paper presented at the Fourth International Symposium on Frontiers of Electrochemistry (Science & Technology), Madras, India, 14-16 Nov 1989.
2. Rathnamma, D. V. and R. Nagarajan, "High Temperature Hot corrosion Control by Fuel additives (Contaminated Fuels), in: Proc. 10th International congress on Metallic Corrosion, 7-11 Nov 1987, Madras, India, Oxford and IBH Publishing, Vol IV, pp. 3651-3664.
3. Zelenznik, Frank, "Solution Capable Complex Chemical Equilibrium Calculations Program," NASA, Lewis, Cleveland, Ohio (1985).

4. Gokoglu, S. A., B. K. Chen, and D. E. Rosner, "Calculation of Multicomponent Convective Diffusion Deposition Rates From Chemically Frozen Boundary Layer Theory, " NASA CR-168329 (computer program) (1984).
5. Rosner, D. E., B. K. Chen, G. C. Fryburg, and F. J. Kohl, "Chemically Frozen Multicomponent Boundary Layer Theory of Salt and/or Ash Deposition Rates from Combustion Gases," Combustion Science Technology, 20, pp. 87-106 (1979).
6. Rosner, D.E. and R.Nagarajan, "Vapor Deposition and Condensate Flow on Combustion Turbine Blades: Theoretical Model to Predict/Understand Some Corrosion Rate Consequences of Molten Alkali Sulfate Deposition in the Field or Laboratory," Int.J.Turbo Jet Engines, 1987.
7. Luthra, K. L. and H. S. Spacil, "Impurity Deposits in Gas Turbines From Fuels Containing Sodium and Vanadium," J. Electrochem.Soc.129 (1982) pp. 649-656.
8. Shores, David A., "New Perspectives on Hot Corrosion Mechanisms," pp. 493-501, NACE-6, 1983. Ed R.A.Rapp.
9. Rosner, D. E. and R. Nagarajan, "Transport-Induced Shifts in Condensate Dew-Point and Composition i Multicomponent Systems With Chemical Reaction," Chem.Eng.Sci.,40,pp. 177-186 (1985).
10. Nagarajan, R., "Theory of Multicomponent Chemical Vapor Deposition (CVD) Boundary Layers and Their Coupled Deposits," Ph.D. Thesis, Chemical Engineering Department, Yale University (May 1986).
11. Natesan, K., "Oxidation-Sulfidation Behavior of Nickel-Base Superalloys and M-Cr-Al Coatings," Materials Science Eng., 87, pp. 9-106 (1987).
12. Cook, L. P. and D. W. Bonnell, "Model for Molten Salt Corrosion of (Co,Cr)-Based Superalloys," NBSIR 87-3628, Final Report Prepared for the Department of the Navy-DTRC by the National Bureau of Standards (Dec 1987).
13. Annen, K. D., "Preparation of a Vanadate Thermodynamic Data Base," JANA-NEW, Final Report Prepared for the Department of the Navy-DTRC by Aerodyne Research, Inc., Billerica, Mass. (1985).
14. Gordon, S. and B. J. McBride, "Calculation of Complex Chemical Equilibrium Compositions, Rocket Performance, Incident and Reflected Shocks, and Chapman-Jouguet Detonations," NASA SP-273 (computer program), interim revision (Mar 1976).

Table 1. Impurity concentrations in three Navy test fuels.

| Impurity           | Fuel  |       |      |
|--------------------|-------|-------|------|
|                    | GT 10 | GT 12 | NSFO |
| Sodium (wt. ppm)   | 1     | 2     | 22   |
| Vanadium (wt. ppm) | -     | 5     | 170  |
| Sulfur (wt. %)     | 1     | 2     | 2    |
| Nickel (wt. ppm)   | -     | -     | 34   |
| Zinc (wt. ppm)     | -     | -     | 2    |
| Iron (wt. ppm)     | -     | -     | 11   |

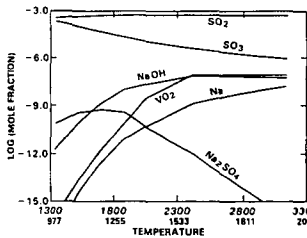


Fig. 1. CEC-predicted vapor phase composition; fuel GT 12, pressure = 1 atmosphere, fuel/air = 1/30.

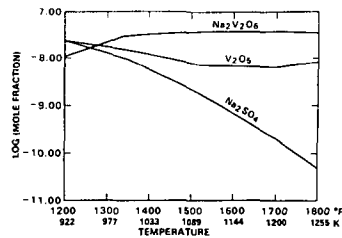


Fig. 2. CEC-predicted liquid phase composition; fuel GT 12, pressure = 1 atmosphere, fuel/air = 1/30.

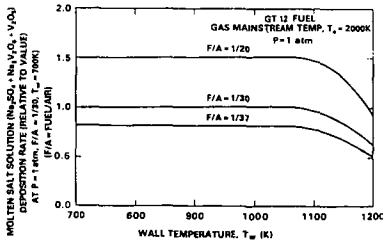


Fig. 3. CFBL deposition rate calculations; predicted dependence on fuel/air (F/A) ratio and blade surface temperature  $T_w$  (K).

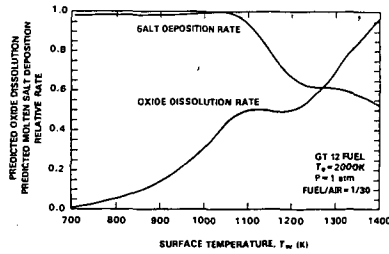


Fig. 4. Predicted effect of blade surface temperature on molten salt deposition and relative oxide (NaO) dissolution rates.

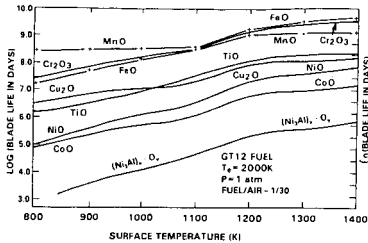


Fig. 5. Predicted hot corrosion-limited life of oxide-coated turbine blades; effect of surface temperature changes.

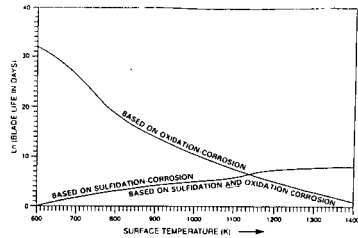


Fig. 6. Predicted surface temperature dependence of  $\text{Cr}_2\text{O}_3$ -coated blade life limited by sulfidation, oxidation, and a combination of the two; fuel GT 12,  $T_s = 2,000 \text{ K}$ ,  $P = 1 \text{ atm}$  atmosphere, fuel/air = 0.0333.

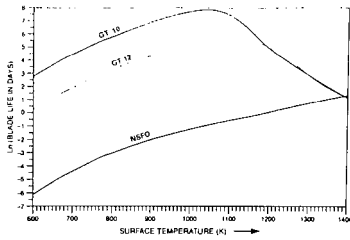


Fig. 7. Evaluation of three heavy test fuels with respect to their corrosion potential; protective coating  $\text{Cr}_2\text{O}_3$ ; fuel: GT 10, GT 12, NSFO,  $T_s = 2,000 \text{ K}$ ,  $P = 1 \text{ atmosphere}$ , fuel/air = 0.0333.

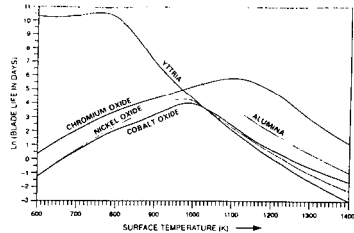


Fig. 8. Computed surface temperature dependence of corrosion-limited life of blades coated with several pure metallic oxides; fuel GT 12,  $T_s = 2,000 \text{ K}$ ,  $P = 1 \text{ atmosphere}$ , fuel/air = 0.0333.

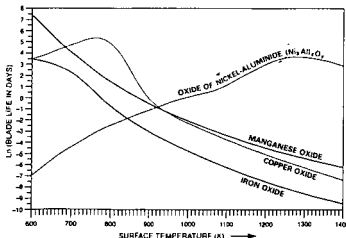


Fig. 9. Predicted surface temperature dependence of corrosion-limited life of blades coated with several metallic and alloy oxides; fuel GT 12,  $T_s = 2,000 \text{ K}$ ,  $P = 1 \text{ atmosphere}$ , fuel/air = 0.0333.

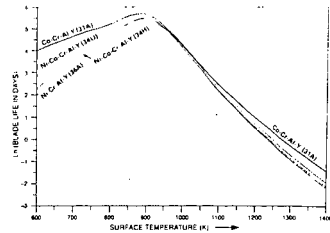


Fig. 10. Predicted surface temperature dependence of corrosion-limited life of blades coated with typical protective alloys; fuel GT 12,  $T_s = 2,000 \text{ K}$ ,  $P = 1 \text{ atmosphere}$ , fuel/air = 0.0333.